

UNSTEADY STAGNATION POINT FLOW WITH PARTIAL SLIP

SHABAN MUSEH

(UDS/MM/0034/14)



2016

UNIVERSITY FOR DEVELOPMENT STUDIES

UNSTEADY STAGNATION POINT FLOW WITH PARTIAL SLIP

BY

SHABAN MUSEH (B.Sc. Mathematics)

(UDS/MM/0034/14)

THESIS SUBMITTED TO THE DEPARTMENT OF MATHEMATICS, FACULTY
OF MATHEMATICAL SCIENCES, UNIVERSITY FOR DEVELOPMENT
STUDIES, IN PARTIAL FULFILMENT OF THE REQUIREMENTS FOR THE
AWARD OF A MASTER OF SCIENCE DEGREE IN MATHEMATICS

JULY, 2016



DECLARATION

Student

I hereby declare that this thesis is the result of my own original work and that no part of it has been presented for another degree in this university or elsewhere.

Candidate's Signature:..... Date:.....

Name: ShabanMuseh

Supervisor

I hereby declare that the preparation and presentation of this thesis was supervised in accordance with the guidelines on supervision of thesis laid down by the University for Development Studies.

Principal Supervisor's Signature:..... Date:.....

Name: Ing. Dr. Ibrahim YakubuSeini



ABSTRACT

The no-slip boundary condition at a solid-liquid interface is primarily to understanding fluid mechanics. However, this condition is an assumption that cannot be derived from first principles and could, in theory, be violated. In this work, we investigate numerically and theoretically the subject involving partial slip boundary conditions. The physical imagery that emerges is that of a complex behaviour at an unsteady hydromagnetic stretching solid interface, with stagnation point flow involving an interplay of many physico-chemical parameters of practical importance, including buoyancy forces informed by the orientation of the stretching sheet, unsteadiness of the flow, radiation effects, viscous dissipation, the partial slip effects, chemical reaction, mass diffusion, momentum diffusion, Lorentz force induced by the magnetic field and the velocity ratio. It is concluded that for this particular flow, the combined effects of these physico-chemical parameters are major determinants of the flow properties and must be carefully controlled to achieve desired results in practice.



ACKNOWLEDGEMENT

My first and foremost gratitude goes to the Almighty Allah for giving me the courage and strength throughout these two years of study leading to this dissertation. He is the most powerful, compassionate, kind and merciful. Secondly, my heartfelt thanks go to my supervisor Ing. Dr. Ibrahim YakubuSeini for his tireless effort, tolerance, patience and dedicated supervision from the beginning of this thesis to this end. His genuine concern and friendship are irreplaceable. My thanks are also due to Dr. Mohammed MuniruIddrisu, the Head of Department for Mathematics for his fatherly advice and encouragement. My regard goes to all lecturers who shared their knowledge with me in the cause of my study. Their contribution to imparting knowledge to me is much appreciated. Finally, my profound appreciation goes to all my course mates and friends who have contributed in diverse ways to my success. God bless you all.



DEDICATION

This work is dedicated to my beloved parents;

UNIVERSITY FOR DEVELOPMENT STUDIES



DECLARATION	I
ABSTRACT.....	II
ACKNOWLEDGEMENTS.....	III
DEDICATION.....	IV
TABLE OF CONTENT.....	V
LIST OF TABLES	IX
LIST OF FIGURES	X
NOMENCLATURE	XII
CHAPTER ONE	1
INTRODUCTION	1
1.1.Modes of Heat Transfer.....	2
1.2.Classification of Flow Pattern	3
1.3.Viscosity and No-Slip Effect.....	4
1.4.Problem Statement	6
1.5 Research Objectives	7
1.5.1 Main Objective	7
1.5.2 Specific Objectives	7
1.6.Significance of the Research	7
1.7.Computational Approach	8



www.udsspace.uds.edu.gh	
1.8.Organisation of Report	8

CHAPTER TWO	9
--------------------------	----------

LITERATURE REVIEW	9
--------------------------------	----------

2.1 MHD Boundary layer flows	9
------------------------------------	---

2.2 Stagnation Point Flows.....	11
---------------------------------	----

CHAPTER THREE	16
----------------------------	-----------

UNSTEADY STAGNATION POINT FLOW WITH PARTIAL SLIP ON A VERTICAL SURFACE	16
---	-----------

3.1 Mathematical formulation of unsteady stagnation point flow	16
--	----

3.1.1 The Continuity Equation	18
-------------------------------------	----

3.1.3. The Momentum Equation	19
------------------------------------	----

3.1.3 The Energy Equation	20
---------------------------------	----

3.1.4 The Concentration Equation	21
--	----

3.1.5 Associated Boundary Conditions	22
--	----

3.2 Self-Similar Solutions	22
----------------------------------	----

3.3 The Similarity Variable	23
-----------------------------------	----

3.4 The Stream Function	25
-------------------------------	----

3.5 Transformation of the Problem	26
---	----

3.5.1 The Continuity Equation	27
-------------------------------------	----

3.5.2 The Dimensionless Momentum Equation	28
---	----





3.5.3 Dimensionless Energy Equation	28
3.5.4 Dimensionless Concentration Equation.....	30
3.5.5 Dimensionless Boundary Conditions	31
3.6.Dimensionless Fluxes.....	32
3.6.1 The Skin Friction Coefficient	32
3.6.2.The Rate of Heat Transfer Coefficient	33
3.6.3 The Rate of Mass Transfer Coefficient	35
CHAPTER FOUR	37
RESULTS AND DISCUSSIONS	37
4.1 Numerical Procedure.....	37
4.2. Validation of Results	38
4.3. Numerical Results	Error! Bookmark not defined.
4.4 Graphical Results	42
4.4.1. Velocity Profiles	42
4.4.2. Temperature Profiles	45
4.4.3 Concentration Profiles	51
CHAPTER FIVE	57
CONCLUSIONS AND RECOMMENDATIONS	57
5.1.Conclusion.....	Error! Bookmark not defined.
5.2.Recommendations	59



REFERENCES	www.udsspace.uds.edu.gh	59
APPENDIX I		69
Derivation of Continuity		69
APPENDIX II		73
Derivation of Momentum Equation		73
APPENDIX III.....		78
Derivation of the Energy Equation		78
APPENDIX IV.....		82
Derivation of the Concentration Equation		82
APPENDIX V		87
MAPLE CODE FOR NUMERICAL RESULTS		87
APPENDIX VI.....		89
MAPLE CODE FOR GRAPHICAL RESULTS		89
APPENDIX VII		92
The Runge-Kutta (RK) Method		92
APPENDIX VIII.....		95
Shooting method		95

Table 4.1 Comparison with Ishak et al, (2006), Pal (2009) and Chen (2014).....**Error! Bookmark not defined.**

Table 4.2 Results of skin friction coefficient, Nusselt and Sherwood numbers for various values of Pr , M , β , Ra , Br and Sc39

Table 4.3 Results of skin friction coefficient, Nusselt and Sherwood numbers for various values of Gt , Gc , A , ε , δ , ζ and ξ41.



LIST OF FIGURES

Figure 1.1 Modes of Heat Transfer.....	2
Figure 1.2 (a) Steady Flow (b) Unsteady Flow.....	3
Figure 1.3 Uniform and Non-uniform Flows.....	4
Figure 1.4 No-slip boundary effect of fluid flow.....	5
Figure 3.1 Schematic Diagram of Problem.....	16
Figure 4.1 Velocity profiles for varying values of magnetic parameter (M).....	43
Figure 4.2 Velocity profiles for varying values of thermal Grashof number (Gt).....	43
Figure 4.3 Velocity profiles for varying values of Solutal Grashof number (Gc).....	44
Figure 4.4 Velocity profiles for varying values of velocity ratio parameter (ϵ)	44
Figure 4.5 Velocity profiles for varying values of unsteadiness parameter (A)	45
Figure 4.6 Temperature profiles for varying values of Magnetic parameter (M).....	46
Figure 4.7 Temperature profiles for varying values of Prandtl number (Pr)	47
Figure 4.8 Temperature profiles for varying values of radiation parameter (Ra).....	47
Figure 4.9 Temperature profiles for varying values of Brinkmann number (Br)	48
Figure 4.10 Temperature profiles for varying thermal Grashof number (Gt).....	48
Figure 4.11 Temperature profiles for varying solutal Grashof number (Gc)	49
Figure 4.12 Temperature profiles for varying values of unsteadiness Parameter (A) ..	49
Figure 4.13 Temperature profiles for varying values of Velocity Ratio Parameter (ϵ)	50
Figure 4.14 Temperature profiles for varying values of Velocity slip Parameter (δ)..	50



Figure 4.15 Temperature profiles for varying values of thermal slip Ratio Parameter (ς)	51
Figure 4.16 Concentration profiles for varying values of magnetic parameter (M)	52
Figure 4.17 Concentration profiles for varying values of reaction rate parameter (β)	53
Figure 4.18 Concentration profiles for varying values of Schmidt number (Sc).....	53
Figure 4.19 Concentration profiles for varying values of thermal Grashof number ...	54
Figure 4.20 Concentration profiles for varying values of Solutal Grashof number ...	54
Figure 4.21 Concentration profiles for varying values of unsteadiness parameter (A)	55
Figure 4.22 Concentration profiles for varying values of velocity ratio parameter (ϵ)	55
Figure 4.23 Concentration profiles for varying values of velocity slip parameter (δ)	56
Figure 4.24 Concentration profiles for varying values of solutal slip parameter (ξ)...	56
Figure A1.1 Mass flux through each of the six faces of a control volume of fluid (Çengel and Cimbala (2006)).....	70
Figure A2.1 x-directional surface forces due to stress tensor component of a control volume (Çengel and Cimbala (2006)).....	73
Figure A4.1 A Control volume in a fluid-flow and mass-diffusion field (Lienhard IV and Lienhard (2008))	82



NOMENCLATURE

(x, y)	Cartesian Coordinates
C_s	Plate surface concentration
C_∞	Free stream concentration
C	Fluid chemical species concentration Vector
D	Diffusion coefficient
f	Dimensionless stream function
Nu	Nusselt number
T_∞	Free stream temperature
Sh	Sherwood number
T	Fluid temperature Vector
Pr	Prandtl number
T_s	Plate surface temperature
κ	Thermal conductivity coefficient
Sc	Schmidt number
(u, v)	Velocity components in Cartesian Coordinates
K'	Mean absorption coefficient
Ra	Thermal radiation parameter
B_0	Magnetic field of constant strength
γ	Reaction rate
q_r	Radiative heat flux



Ha_x	Local magnetic field parameter
Br	Brinkmann number
Bi_x	Local Biot number
Sc	Schmidt number
β_x	Local reaction rate parameter
Φ	Viscous dissipation function
q_m	Mass diffusion flux
h_s	Heat transfer coefficient at plate surface

Greek Letters

μ	Coefficient of viscosity
ρ	Density of the fluid
ϕ	Dimensionless concentration
θ	Dimensionless temperature
η	Dimensionless variable
ν	Kinematic viscosity
ψ	Stream function
σ^*	Stefan-Boltzmann constant
σ	Fluid electrical conductivity



CHAPTER ONE

INTRODUCTION

Heat transfer continues to receive considerable attention from the scientific research community because of its numerous industrial applications in many fields of engineering such as mechanical, chemical and process engineering. In addition, civil engineers, construction engineers and environmental control engineers need considerable knowledge of the subject of heat transfer to design systems that are not only conducive for habitation but resilient over a period of time.

In thermal power plants, boilers and condensers are designed in such a way that the desired rate of heat transfer can be achieved. A Bessemer converter for making steel from pig iron must be designed so that it provides sufficient opportunity for the carbon to be oxidized quickly enough for the process to be economical (Mitchell 1950). An artificial kidney must have sufficient capacity to remove the toxins from the blood. Furthermore, knowledge of heat transfer processes is required in the design of electronic components to ensure that the incidence of overheating is curtailed (Sathyanarayanan and Ramprabhu, 2005).



1.1. Modes of Heat Transfer

There are three basic modes by which heat can be transferred. These include conduction, radiation, and convection.

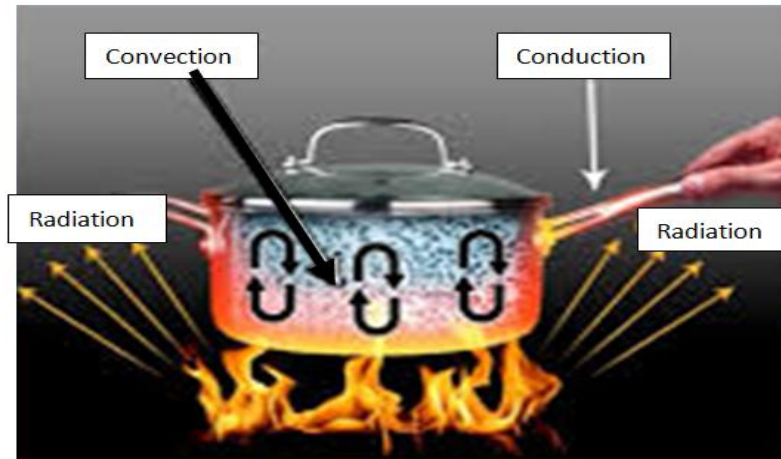


Figure1.1 Modes of Heat Transfer (www.spectrose.com)

Conduction

Conduction is an exchange of energy by direct interaction between molecules of a substance having temperature difference (See Figure 1.1). It occurs in gases, liquids, or solids and has a strong basis in the molecular kinetic theory of Physics.

Radiation

Radiation is a transfer of thermal energy in the form of electromagnetic waves. Liquids containing gases, such as carbon dioxide, water vapour, and glasses transmit only a portion of incident radiation, while most of solids are essentially opaque to radiation.



Convection

Convection is the process of heat transfer from one location to the next by the movement of fluid molecules. Fluid flows from high pressure location to points of low pressure. Convection is the mode of heat transfer between a solid surface and the adjacent fluid that is in motion (See Figure 1.1)

1.2. Classification of Flow Pattern

There are different forms in which fluid flow can be classified, usually characterized by time and distance:

Time: A flow is *steady* if the parameters describing it (such as velocity, pressure, *et cetera*) do not change with time otherwise the flow is *unsteady* (Stonecypher, 2009) (Fluid Dynamics Figure 1.2).

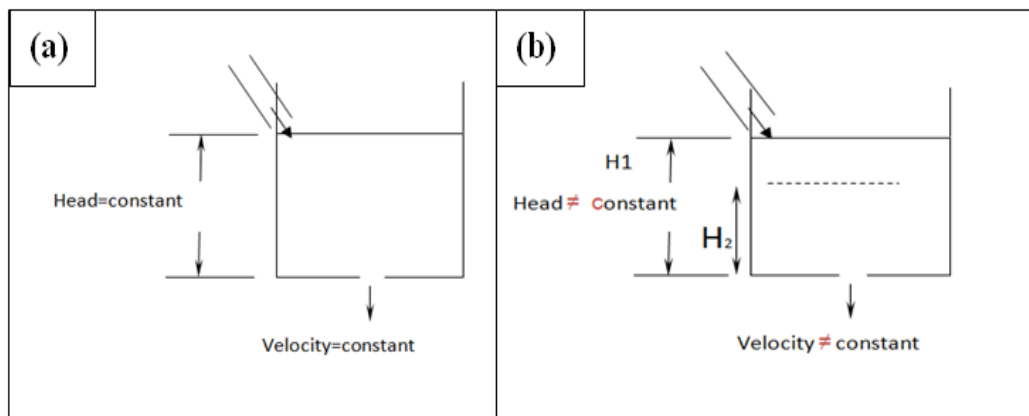


Figure 1.2 (a) Steady Flow (b) Unsteady Flow



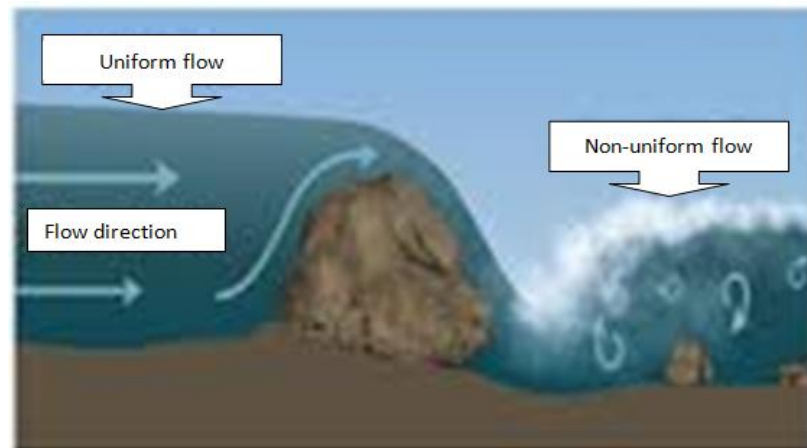


Figure 1.3 Uniform and Non-uniform Flows

(riverrestoration.wikispaces.com/hydraulics)

Distance: A flow is uniform if the parameters describing the flow do not change with distance. In non-uniform flow, the parameters change from point to point along the flow (See Figure 1.3).

From these definitions, almost all flows can be a combination such as *steady uniform* flow, *steady non-uniform* flow, *unsteady non-uniform* flow and *unsteady uniform* flow. Many researches in the field of fluid dynamics have resorted to the steady flow conditions in which time effects are neglected resulting in great simplifications of the analysis of the boundary layer equations. This research considers both the *unsteady uniform* flow condition and the partial slip conditions.

1.3. Viscosity and No-Slip Effect

When two fluid layers move relative to each other, frictional forces develop between them with the slower layer tending to slow down the faster layer. This internal



resistance to flow is quantified by the fluid property *viscosity*, which is a measure of internal stickiness of the fluid.

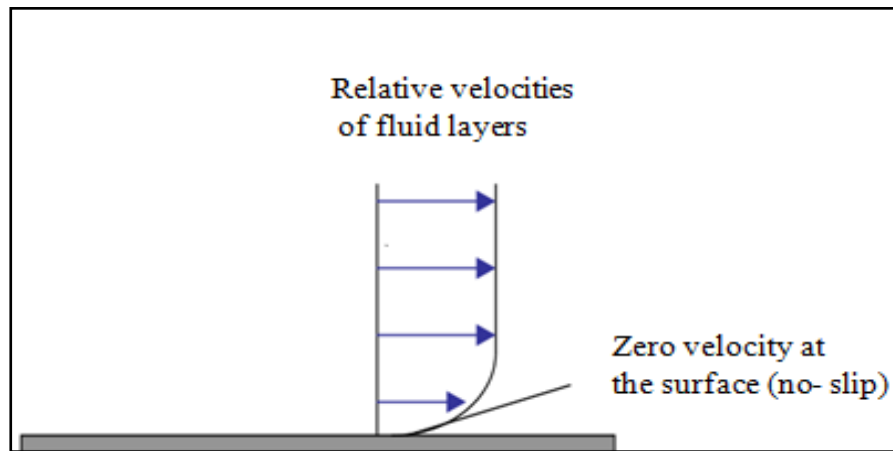


Figure 1.4 No-slip boundary effect of fluid flow

Viscosity is caused by cohesive forces between the molecules in liquids and by molecular collisions in gases. There is no known fluid with zero viscosity, thus all fluid flows involve viscous effects to some degree. Flows in which the frictional effects are significant are called viscous flows.

Due to viscosity, many experiments have concluded that fluid molecules in motion are halted at the surface and assume a zero velocity relative to the surface. This means that, a fluid in direct contact with a solid “sticks” to the surface due to viscous effects. This is known as the *no-slip* condition (Engineering Archives). However, in many flows of practical relevance, there are regions where viscous forces are negligibly small compared to inertial or pressure forces. The assumption that the flow field obeys the conventional no-slip condition at the boundary is no longer valid as *partial slip* boundary condition has become dominant in most situations (Andersson, 2002).



With a slip at the wall boundary, the shear stress in the fluid is quite different from those in the no-slip cases.

Furthermore, it is desired to design shapes of cast-iron components to provide for uniform cooling, and for fabrication processes of semi-conductors (Gupta,2008). Due to its diverse applications in thermodynamics, material science, diffusion theory, fluid mechanics, and radiation theory, heat transfer is termed the “heart” of thermal engineering.

1.4. Problem Statement

The combined effects of thermo physical properties of fluid on stagnation-point flow due to a stretching surface is a major concern to the scientific research community due to its importance and practical relevance. The introduction of this flow by Hiemenz(1911) in the early twentieth century attracted the interest of many researchers to stagnation-point flow. The available literature admits the well-known no-slip boundary conditions. The assumption of no slip at the boundary, though simplifies complicated fluid flow regimes for analysis, is ideal in the case of stretching sheet and will rarely apply in practical engineering systems. With a slip at the wall boundary, the flow behaviour and the shear stress in the fluid are quite different from that of no-slip case. Motivated by this, the research aims to study the behaviour of unsteady stagnation-point flow towards a stretching sheet with slip effect at the boundary.



1.5 Research Objectives

1.5.1 Main Objective

The main objective of the study is to analyse the time-dependent stagnation-point flow over a vertical surface with partial slip effects.

1.5.2 Specific Objectives

- i. To develop a mathematical representation of unsteady stagnation point flow with partial slip at the surface.
- ii. To apply similarity techniques to transform the modelled partial differential equations to ordinary differential equations which are amenable to numerical techniques.
- iii. To determine which parameters are critical in the control of unsteady stagnation point flow with partial slip.

1.6. Significance of the Research

This study is significant in many respects including but not limited to:

- i. Engineers in the design of effective and efficient heat exchanger components.
- ii. Biomedical engineers to produce lasers for medical applications in which the cooling rate can be controlled to avoid irreversible damages to cells.
- iii. Manufacturing industries to cool their finished products efficiently.
- iv. Adds up to existing literature and serves as a reference material for other future researchers.



1.7. Computational Approach

The differential equations describing the unsteady stagnation point boundary layer flow interaction with partial slip constitute a nonlinear problem in an unbounded computational domain. Nonlinear differential equations can adequately model practical engineering problems whose solutions are amenable to numerical techniques. The most common numerical methods employed by researchers include: the Runge-Kutta Method, Finite Difference Method, Perturbation Method, the Shooting Method, and the Keller Box method. All these methods provide solutions to the accuracy required for most engineering applications. In this study, the Runge-Kutta method alongside the Newton Raphson shooting techniques shall be applied. This is because they are easy to implement and are very stable. The model shall be run on Maple 16 software to generate numerical and graphical results for analysis.

1.8 Organisation of Report

This dissertation is organised into five chapters. Chapter one presents the introduction. The problem is stated and the research methodology outlined. In Chapter Two, related literature is reviewed. Chapter Three applies the formulae to solving the problem. Chapter Four presents the results and discussions whilst Chapter Five concludes the report with some recommendations for future researchers.



LITERATURE REVIEW

Heat transfer is energy in transit, which occurs as a result of temperature gradient or differences. This temperature difference is thought of as a driving force that causes heat to flow. The three basic mechanisms of heat transfer are convection, conduction and radiation, which may occur separately, or simultaneously. The subject matter of this research is solely based on the individual mechanism of free convection and radiation.

Free convective heat transfer is an inevitable phenomenon in engineering systems due to its diverse applications in electronic cooling, heat exchanger designs and thermal systems. Studies pertaining to coupled heat and mass transfer due to free convection have wide applications in different realms, such as, mechanical, geothermal, chemical sciences, etc. Many industrial and technological setups such as nuclear reactors, food processing, and polymer production experience not only temperature difference but concentration. The chemical concentration variation ultimately affects the rate of heat transfer.

2.1 MHD Boundary layer flows

Chamkha (2004) investigated unsteady MHD convective heat and mass transfer past a semi-infinite vertical permeable moving plate with heat absorption. He solved the dimensionless governing equations using two-term harmonic and non-harmonic functions and observed that when the solutal Grashof number was increased, the concentration buoyancy effects were enhanced and thus, the fluid velocity increased.





www.udsspace.uds.edu.gh

He further observed the correlation between the Nusselt number, the heat absorption coefficient as well as Sherwood number and the Schmidt number. Makinde (2010) produced similarity solutions of hydromagnetic heat and mass transfer over a vertical plate with convective surface boundary conditions. He observed that the local skin-friction coefficient, as well as the local heat and mass transfer rate at the plate surface increase with increasing intensity of the magnetic field, buoyancy forces and convective heat exchange parameters.

Abdel-Khalek (2009) examined MHD free convection flow with mass transfer from a moving permeable vertical surface and produced interesting results using the perturbation techniques. Mohd. *et al* (2015) investigated the MHD stagnation-point flow and heat transfer with effects of viscous dissipation, joule heating and partial velocity. Aurg (2015) studied the slip effect of an unsteady MHD stagnation-point flow of a micropolar fluid towards a shrinking sheet with thermophoresis effect and observed that the concentration boundary layer thickness decreased with increasing values of the thermophoresis parameter. Auran *et al.* (2016) investigated the effect of partial slip on an unsteady MHD mixed convection stagnation-point flow of a micropolar fluid towards a permeable shrinking sheet. Hayat and Nawaz (2016) then investigated the MHD stagnation-point flow of an upper-convected Maxwell fluid over a stretching surface.

2.2 Stagnation Point Flows

The problem of stagnation-point flow of fluid due to a stretching sheet is a major concern for researchers because of its practical applications in metallurgy and chemical engineering fields. Extrusions of polymers, glass fibre, the cooling of metallic plate are some specific applications in practice. Hiemenz (1911) examined the two-dimensional stagnation flow in his first work by using similarity transformations to reduce the Navier–Stokes equations to non-linear ordinary differential equations. The result was later extended to the axisymmetric case by Homann (1936) and improved by Howarth (1938). Following these works, various aspects of stagnation-point flow and heat transfer have been studied as available in literature. (see Chiam, 1994; Mahapatra and Gupta, 2002; Layek *et al.*, 2007; Ishaket *et al.*, 2008; Bhattacharyya *et al.*, 2012, Bhattacharyya and Vajravelu, 2012; and Arthur and Seini, 2014). The flow becomes time dependent in certain aspects, but the physical situation described in the above studies is under the condition of a steady state. Fauzi *et al.* (2015) analysed the stagnation point flow and heat transfers over a nonlinear shrinking sheet with slip effects. It was observed that the slip - velocity delays the boundary layer separation whereas the temperature slip does not affect the boundary layer separation. Khairy and Anuar (2016) investigated the stagnation-point flow towards a Stretching Vertical Sheet with Slip Effects. It is found that dual solutions exist in a certain range of slip and buoyancy parameters.



2.3 Unsteady Stagnation Point Flows on Flat Surfaces

Few researchers have attempted the investigations into the unsteadiness of flow problems. Nazaret *et al.* (2004) studied the unsteady boundary layer flow in the region of stagnation points on a stretching sheet, while Bhattacharyya (2011) investigated the unsteady stagnation point flow over a shrinking sheet. Sharma and Singh (2008) analysed the unsteady flow near a stagnation point on a stretching sheet in the presence of a time-dependent free stream. Some important properties of unsteady flows on a stretching sheet were described in the works of Bachoket *et al.* (2011), Ishaket *et al.* (2009), and Hayat *et al.* (2010). Slip Mixed convection in stagnation point flow is of significance in fluid mechanics when the buoyancy forces due to the temperature difference between the surface and the free stream become large, in the sense that both the flow and thermal fields are greatly affected by the buoyancy forces. Devi *et al.* (1991) studied the unsteady laminar mixed convection in two-dimensional stagnation-point flows around heated surfaces by taking both cases of an arbitrary wall temperature and arbitrary surface heat flux variations. The unsteady mixed convection flow of a micro polar fluid was studied by Loket *et al.* (2006) who found the smooth transition from the initial unsteady-state flow to the final steady-state flow. Ishaket *et al.* (2010) reported the existence of dual solutions for both assisting and opposing flows of an electrically conducting fluid past a vertical permeable flat plate. Hayat *et al.* (2012) investigated the effects of mixed convection unsteady stagnation point flow over a stretching sheet with heat transfer in the presence of variable free stream. Kohilavani *et al.* (2015) studied the unsteady stagnation point flow and heat transfer of a special third grade fluid past a permeable stretching/shrinking





www.udsspace.uds.edu.gh

sheet. Results from the stability analysis depict that the first solution (upper branch) is stable and physically realizable, while the second solution (lower branch) is unstable. Hui (2015) investigated the mixed convection unsteady stagnation-point flow towards a stretching sheet with slip effects. The numerical results show that the increase of unsteadiness parameter and the slip effects cause increment in the existence range of similarity solution. The effects of unsteadiness parameter, the velocity ratio parameter, and the velocity and thermal slip parameters on the velocity and temperature distributions are analysed and discussed.

Niket *et al.* (2016) investigated the unsteady stagnation point flow and heat transfer over a stretching/shrinking sheet and concluded that dual solutions exist for the shrinking case while for the stretching case, the solution was unique. Moreover, it is found that the heat transfer rate at the surface increases as the stretching/shrinking parameter as well as the unsteadiness parameter increases. Khalid *et al.* (2016) investigated the multiple solutions of an unsteady stagnation-point flow with melting heat transfer in a Darcy–Brinkman porous medium whilst Fotini and Daiming (2016) considered the unsteady stagnation-point flow of a second-grade fluid and observed that the effect of the Weissenberg number was to decrease the velocity near the wall as it increases. Malvandi *et al.* (2016) also investigated the slip effects on unsteady stagnation point flow of a nanofluid over a stretching sheet.

2.4 Boundary Layer Flow with Surface Slip

All the studies referred to in the foregoing sections made assumptions of the flow field obeying the conventional no-slip condition at the boundary. Wang (2002) gave an



exact solution of the www.udsspace.uds.edu.gh Navier-Stokes equations for the flow due to a stretching boundary with slip. He later considered the effect of stagnation slip flow on the heat transfer from a moving plate, Wang (2006). Ariel (2008) studied the effects of slip on the flow of an elastic-viscous fluid with some other physical features. Many researchers have contributed to the investigations of slip flows in different configurations (see Fang *et al.*, 2009; Bhattacharyya *et al.*, 2011; Mukhopadhyay and Gorla, 2012; Mukhopadhyay *et al.*, 2012; and Bhattacharyya *et al.*, 2013).

Cao and Baker (2009) considered the slip effects on the mixed convective flow and heat transfer from a vertical plate and reported the local non similarity solutions. Mukhopadhyay (2011) investigated effects of slip on unsteady mixed convective flow and heat transfer past a stretching and a porous stretching surface. Bhattacharyya *et al.* (2013) studied the mixed convective flow adjacent to a vertical permeable stretching sheet in porous media with slip effects. The similarity solution of the mixed convection boundary layer flow near the stagnation-point on a vertical surface with slip effect was studied by Amanet *al.* (2011). Niket *al.* (2013) studied mixed convection boundary layer caused by time-dependent velocity and the surface temperature in the two-dimensional unsteady stagnation-point flow over a stretching vertical sheet with the no-slip boundary condition. Chen (2014) studied mixed convection unsteady stagnation-point flow towards a stretching sheet with slip effects. Noret *al.* (2015) investigated the boundary layer stagnation-point slip flow and heat transfer towards a shrinking, stretching cylinder over a permeable surface. Tapas and Samir (2016) investigated slip effects on unsteady stagnation-point flow and heat transfer over a shrinking sheet.

www.udsspace.uds.edu.gh

This study therefore investigates the unsteady stagnation point flow with partial slip as it approximates closely with real practice in industry.



UNSTEADY STAGNATION POINT FLOW WITH PARTIAL SLIP ON A VERTICAL SURFACE

In this chapter, the unsteady stagnation point flow with partial slip on a vertical surface is modeled. The equations are then transformed from partial differential equations to ordinary differential equations. These equations are then reduced to first order system of ordinary differential equations and solved using the Runge-Kutta method alongside the Newton Raphson shooting techniques.

3.1 Mathematical formulation of unsteady stagnation point flow

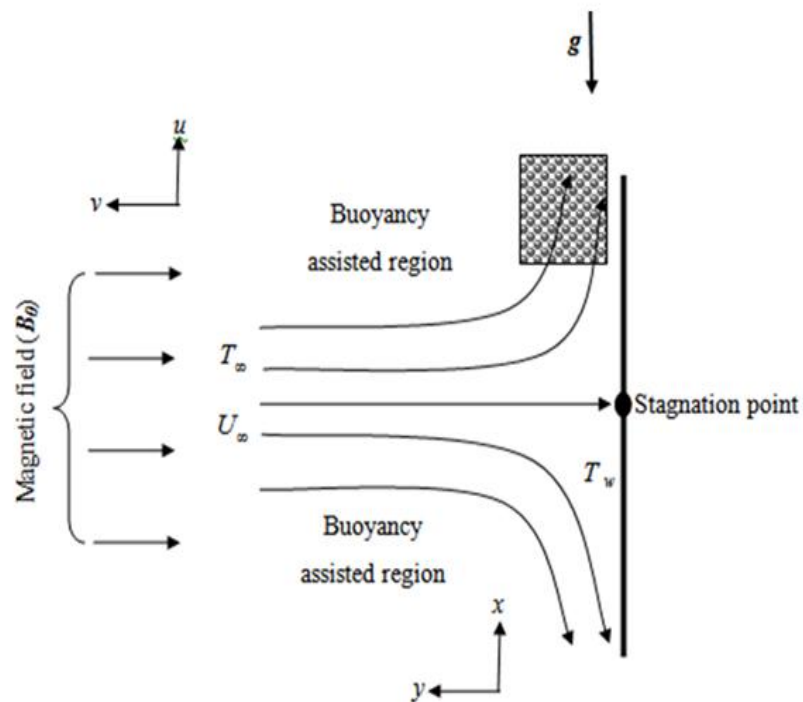


Figure 3.1 Schematic Diagram of Problem

Consider an unsteady two-dimensional stagnation point flow of an incompressible viscous dissipative fluid towards a vertical stretching sheet (see figure 3.1). Let the x -



axis be taken along the direction of the sheet and y -axis normal to it. The flow is subjected to a transverse magnetic field of strength B which is assumed to be applied in the positive y -direction, normal to the surface. The tangential velocity U_s , due to the stretching surface is assumed to vary proportionally to the distance x so that $U_s = ax/(1-ct)$, where c is a parameter showing the unsteadiness of the problem and a is a constant with $a > 0$ for a stretching sheet. The free stream velocity is $U_\infty = bx/(1-ct)$, where $b > 0$ is the strength of the stagnation flow. The surface temperature T_s of the stretching sheet varies with the distance x as $T_s = T_\infty + T_0 x/(1-ct)^2$, where T_∞ is the constant free stream temperature with $T_0 \geq 0$. Also the surface concentration C_s of the stretching sheet varies with the distance x as $C_s = C_\infty + C_0 x/(1-ct)^2$, where C_∞ is the constant free stream concentration with $C_0 \geq 0$.

The particular forms of the above expressions for U_s , U_∞ , T_s and C_s have been chosen in order to transform the governing partial differential equations into a set of ordinary differential equations, thereby facilitating the exploration of the effects of the controlling parameters. It should be noted that the expressions for U_s , U_∞ , T_s and C_s are valid for time $t < c^{-1}$ and a , b , c , have dimension t^{-1} .

If u , v , T and C are the fluid x -component of velocity, y -component of velocity, temperature and concentration respectively. With these assumptions, the governing equations for the problem can be modeled as shown in the sections following:



3.1.1 The Continuity Equation

The continuity of flow for fluids in motion is derived using the mass conservation principles formulated mathematically (See Appendix 1):

$$\frac{D\rho}{Dt} + \rho \nabla \cdot V = 0 \quad (3.1)$$

Consider the substantial derivative

$$\frac{D}{Dt} = \frac{\partial}{\partial t} + \frac{\partial}{\partial x} + \frac{\partial}{\partial y} + \frac{\partial}{\partial z} \quad (3.2)$$

The problem under study is unsteady two- dimensional (no z -axis) so $\frac{\partial}{\partial z} = 0$. Hence

(3.2) reduces to

$$\frac{D}{Dt} = \frac{\partial}{\partial t} + \frac{\partial}{\partial x} + \frac{\partial}{\partial y} \quad (3.3)$$

The velocity field, $V = u\hat{i} + v\hat{j} + w\hat{k}$ and its divergence, $\nabla = \frac{\partial}{\partial x}\hat{i} + \frac{\partial}{\partial y}\hat{j} + \frac{\partial}{\partial z}\hat{k}$, now

become:

$$V = u\hat{i} + v\hat{j}, \quad \nabla = \frac{\partial}{\partial x}\hat{i} + \frac{\partial}{\partial y}\hat{j} \text{ respectively}$$

$\frac{D\rho}{Dt} = 0$ (Incompressibility of the fluid) and dividing through by ρ , (3.1) becomes

$$\nabla \cdot V = 0$$

The continuity equation given in Equation 3.1 now simplifies to:



$$\frac{\partial u}{\partial x} + \frac{\partial v}{\partial y} = 0 \quad (3.4)$$

3.1.3. The Momentum Equation

From the Navier-Stokes equation (See Appendix II)

$$\rho \frac{DV}{Dt} = -\nabla p + \rho g + \mu \nabla^2 V \quad (3.5)$$

where ρ is the density of the fluid, g is the acceleration due to gravity, p is the external pressure and μ is the dynamic viscosity of the fluid.

For a vertical surface, the force of gravity is important as it produces buoyancy effects in the flow. In a free stream flow, atmospheric pressure applies and hence can be ignored as it is equally distributed in all directions. The Navier – Stokes equation become:

$$\rho \left(\frac{\partial u}{\partial t} + u \frac{\partial u}{\partial x} + v \frac{\partial u}{\partial y} \right) = -\frac{\partial p}{\partial x} + \mu \frac{\partial^2 u}{\partial y^2} + \rho g, \quad (3.6)$$

The presence of the transverse magnetic field produces the Lorenz force which tends to impede the velocity of flow. Charged particles moving with the fluid will experience an induced electric field, $V \times B_0$ which will tend to drive an electric current in the direction perpendicular to both V and B_0 . Neglecting the Hall Effect, the magnitude of the current density for a weakly ionized fluid is given by the generalized Ohm's law as;

$$j = \sigma(-V \times B_0) \quad (3.7)$$



For the purposes of this study, both V and σ are assumed to be uniform. In terms of the two dimensional coordinate system:

$$j = \sigma B_0 u \quad (3.8)$$

Movements of a conducting material in a magnetic field generate electric currents j , which in turn induces a magnetic field. Each unit volume of liquid having j and B_0 experiences MHD force $j \times B_0$, known as the “Lorenz force” which retards the motion of the flow:

$$j \times B_0 = \sigma B_0^2 u \quad (3.9)$$

Therefore, including the stagnation pressure $-\frac{\partial p}{\partial x} = \frac{\partial U_\infty}{\partial t} + U_\infty \frac{\partial U_\infty}{\partial x}$, and magnetic force into the flow field reduces the momentum of the flow as given in Equation in 3.6 to:

$$\frac{\partial u}{\partial t} + u \frac{\partial u}{\partial x} + v \frac{\partial u}{\partial y} = \frac{\partial U_\infty}{\partial t} + U_\infty \frac{\partial U_\infty}{\partial x} + \nu \frac{\partial^2 u}{\partial y^2} + g\beta_t(T - T_\infty) + g\beta_c(C - C_\infty) - \frac{\sigma B_0^2}{\rho} u \quad (3.10)$$

Equation 3.10 models the momentum equation for the problem under study.



3.1.3 The Energy Equation

The energy conservation equation for incompressible viscous fluid flow is derived in Appendix III as

$$\frac{DT}{Dt} = \alpha \Delta^2 T + \Phi \quad (3.11)$$

Where,

$$\Phi = 2\mu \left[\left(\frac{\partial u}{\partial x} \right)^2 + \left(\frac{\partial v}{\partial y} \right)^2 + \left(\frac{\partial w}{\partial z} \right)^2 + \frac{1}{2} \left(\frac{\partial u}{\partial y} + \frac{\partial v}{\partial x} \right)^2 + \frac{1}{2} \left(\frac{\partial v}{\partial z} + \frac{\partial w}{\partial y} \right)^2 + \frac{1}{2} \left(\frac{\partial u}{\partial z} + \frac{\partial w}{\partial x} \right)^2 \right]$$

The left hand side of (3.11) represents the convective term whilst the right hand side are respectively, the rate of heat diffusion to the fluid particles and the rate of viscous dissipation per unit volume.

Thus, (3.11) can be expanded as

$$\frac{\partial T}{\partial t} + \left(u \frac{\partial T}{\partial x} + v \frac{\partial T}{\partial y} + w \frac{\partial T}{\partial z} \right) = \alpha \left(\frac{\partial^2 T}{\partial x^2} + \frac{\partial^2 T}{\partial y^2} + \frac{\partial^2 T}{\partial z^2} \right) + \Phi \quad (3.12)$$

For a two dimensional unsteady stagnation point flow with magnetic field and radiative heat flux, results (3.12) is modified to become:

$$\frac{\partial T}{\partial t} + u \frac{\partial T}{\partial x} + v \frac{\partial T}{\partial y} = \alpha \frac{\partial^2 T}{\partial y^2} + \frac{\nu}{c_p} \left(\frac{\partial u}{\partial y} \right)^2 + \frac{\sigma B^2}{\rho c_p} u^2 - \frac{\alpha}{\kappa} \frac{\partial q_r}{\partial y} \quad (3.13)$$

3.1.4 The Concentration Equation

The chemical species concentration equation is derived in Appendix IV as

$$\frac{DC}{Dt} = \mathcal{D} \nabla^2 C \pm \dot{r}, \quad (3.14)$$

where C is the species concentration, \mathcal{D} is the mass diffusivity and \dot{r} is the rate of species generation or destruction.

Substituting the component forms of species concentration, (3.14) reduces to



$$\frac{\partial C}{\partial t} + u \frac{\partial C}{\partial x} + v \frac{\partial C}{\partial y} = \mathcal{D} \frac{\partial^2 C}{\partial y^2} - \gamma(C - C_\infty) \quad (3.15)$$

In Equation 3.15, the negative reaction rate parameter (γ) signifies the rate of species destruction.

3.1.5 Associated Boundary Conditions

The associated boundary conditions for the problem are required to enable a complete solution. With $L = l\sqrt{1 - ct}$ as the velocity slip factor; $M = m\sqrt{1 - ct}$, as thermal slip factor and $N = n\sqrt{1 - ct}$, as the solutal slip factor, where l , m and n are the initial values of velocity, thermal and solutal slip factors, respectively, the boundary conditions with partial slip are given by:

$$\begin{aligned} y = 0: \quad u &= U_s + L\nu \frac{\partial u}{\partial y}, \quad v = 0, \quad T = T_s + M \frac{\partial T}{\partial y}, \quad C = C_s + N \frac{\partial C}{\partial y}, \\ y \rightarrow \infty: \quad u &= U_\infty, \quad T = T_\infty, \quad C = C_\infty, \end{aligned} \quad (3.16)$$

3.2 Self-Similar Solutions

The similarity solution is based on the idea that the velocity, temperature and species concentration distributions at any point along the plate surface, x , will collapse if they are plotted in dimensionless form as a function of an appropriately defined similarity variable. The similarity variable is defined as the ratio of the distance from the plate surface (y) to the approximate thickness of the momentum boundary layer (δ_m):



$$\eta = \frac{y}{\delta_m} \quad (3.17)$$

Therefore, the partial differential equations that describe the problem in terms of x and y will collapse to ordinary differential equations in η for dimensionless velocity, dimensionless temperature and dimensionless species concentration.

3.3 The Similarity Variable

The growth of the velocity, thermal and concentration boundary layers in a laminar flow occur primarily due to the molecular diffusion of momentum and energy. Therefore, the momentum boundary layer thickness (δ_m) will grow approximately according to:

$$\delta_m \approx 2\sqrt{\nu t} \quad (3.18)$$

where ν is the kinematic viscosity and t is time, which is related to the distance from the leading edge (x) and the characteristic velocity (u_{char}) according to:

$$t = \frac{x}{u_{char}} \quad (3.19)$$

For this study, the length is the total length of the plate (which is taken along the x -axis) while the characteristic velocity is the constant free-stream velocity far away from the plate (U_∞).

Substituting (3.18) into (3.19) leads to:

$$\delta_m \approx 2\sqrt{\frac{\nu x}{u_{char}}} \quad \text{when } u_{char} = u_\infty$$



$$\text{we have } \delta_m \approx 2 \sqrt{\frac{vx}{u_\infty}} \quad (3.20)$$

Substituting (3.20) into (3.17) gives:

$$\eta = \frac{y}{2} \sqrt{\frac{U_\infty}{vx}} \quad (3.21)$$

Following the presentation of Ostrach (1953), the constant used to define the similarity parameter is adjusted slightly and from the assumptions that

$U_\infty = bx/(1-ct)$, (3.21) becomes,

$$\eta = y \sqrt{\frac{b}{(1-ct)v}} \quad (3.22)$$

Hence (3.22) defines the similarity variable for the problem under investigation. The dimensionless velocity, temperature and concentration are obtained from:

$$f' = \frac{u}{U_\infty} \quad (3.23)$$

$$\theta = \frac{T - T_\infty}{T_s - T_\infty} \quad (3.24)$$

$$\phi = \frac{C - C_\infty}{C_s - C_\infty} \quad (3.25)$$

At any position, x will collapse when expressed in terms of (3.22). Therefore,

$$f' = f'(x, y) = f'(\eta) \quad (3.26)$$



$$\theta = \theta(x, y) = \theta(\eta) \quad \frac{\text{www.udsspace.uds.edu.gh}}{(3.27)}$$

$$\phi = \phi(x, y) = \phi(\eta) \quad (3.28)$$

3.4 The Stream Function

The stream function is defined such that the continuity equation is satisfied automatically. That is,

$$u = \left(\frac{\partial \psi}{\partial y} \right)_x \text{ and } v = - \left(\frac{\partial \psi}{\partial x} \right)_y \quad (3.29)$$

The stream function is related to the volumetric flow Q , between the surface of the plate and any position y according to,

$$Q = W\psi, \quad (3.30)$$

Where W is the width of the plate. The volumetric flow rate is calculated from the velocity according to:

$$Q = W \int_0^y u \, dy \quad (3.31)$$

Equation 3.31 can be expressed in terms of the dimensionless variables (f' and η)

$$Q = W U_\infty \sqrt{\frac{ux}{U_\infty}} \int_0^\eta f' \, d\eta \quad (3.32)$$

Substituting (3.32) into (3.30) leads to:



$$\psi = U_{\infty} \sqrt{\frac{ux}{U_{\infty}}} \int_0^{\eta} f'(\eta) d\eta \quad (3.33)$$

The integral $\int_0^{\eta} f'(\eta) d\eta = f(\eta)$ in Equation 3.33 can be thought of as the dimensionless form of the stream function and it must be a function of only the similarity variable (η). Simplifying and using $U_{\infty} = bx/(1-ct)$ from the assumptions, Equation 3.33 becomes:

$$\psi = \sqrt{\frac{bx^2\nu}{1-ct}} f(\eta) \quad (3.34)$$

The stream function in Equation 3.34 can be rewritten as:

$$\psi = x \sqrt{\frac{b\nu}{1-ct}} f(\eta) \quad (3.35)$$

3.5 Transformation of the Problem

The similarity variables are now substituted into the governing partial differential equations as well as the boundary conditions to obtain three coupled ordinary differential equations that can be solved more easily. The continuity equation is automatically satisfied using the stream function as defined. The transformation process involves taking the problem in terms of x and y and re-stating it in terms of η .

The similarity variable is differentiated with respect to x, y and t as.

$$\frac{\partial \eta}{\partial x} = 0, \quad \frac{\partial \eta}{\partial y} = \sqrt{\frac{b}{\nu(1-ct)}}, \quad \text{and} \quad \frac{\partial \eta}{\partial t} = \frac{1}{2} c(1-ct)^{-\frac{3}{2}} y \sqrt{\frac{b}{\nu}} \quad (3.36)$$



The x - component of velocity (u) is expressed in terms of the similarity variables as:

$$u = x \left(\frac{b}{1-ct} \right) f' \quad (3.37)$$

The y - component of velocity (v) is expressed in terms of the similarity variables as:

$$v = -\frac{\partial \psi}{\partial x} = -f \sqrt{\frac{bv}{1-ct}} \quad (3.38)$$

Simplifying and rearranging (3.38) gives:

$$v = -\sqrt{\frac{bv}{1-ct}} f \quad (3.39)$$

The partial derivatives of u in (3.37) with respect to x , y and t are respectively:

$$\frac{\partial u}{\partial x} = \left(\frac{b}{1-ct} \right) f', \quad \frac{\partial u}{\partial y} = x \sqrt{\frac{b^3}{v(1-ct)^3}} f'', \quad \frac{\partial^2 u}{\partial y^2} = \frac{xb^2}{v(1-ct)} f''' \quad (3.40)$$

$$\frac{\partial u}{\partial t} = \frac{bc}{2} xy \sqrt{\frac{b}{v}} (1-ct)^{-\frac{5}{2}} f'' + bcx(1-ct)^{-2} f'$$

The partial derivative of v in (3.38) with respect to x , y and t are respectively

$$\frac{\partial v}{\partial y} = -\left(\frac{b}{1-ct} \right) f''(\eta) \quad (3.41)$$

3.5.1 The Continuity Equation

The continuity equation (3.4) is satisfied using (3.40) and (3.41).



3.5.2 The Dimensionless Momentum Equation

For the momentum equation, substituting (3.37), (3.39), (3.40) in (3.10) gives,

$$\left[\frac{bcxy}{2} \sqrt{\frac{b}{v}} (1-ct)^{-\frac{5}{2}} f'' + bcx(1-ct)^{-2} f' \right] + \frac{bx}{(1-ct)} f' \left(\frac{b}{(1-ct)} f' \right) + \left(-\sqrt{\frac{bv}{1-ct}} f \right) \left(x \sqrt{\frac{b^3}{v(1-ct)^3}} f'' \right) = bcx(1-ct)^{-2} + \left(\frac{bx}{(1-ct)} \right) \left(\frac{b}{(1-ct)} \right) + \frac{vxb^2}{v(1-ct)^2} f''' + g\beta_t \theta (T_w - T_\infty) + g\beta_c (C_w - C_\infty) - \frac{\sigma B^2}{\rho} x \left(\frac{b}{1-ct} \right) f' \quad (3.42)$$

Expanding brackets, simplifying and rearranging (3.40) gives,

$$f''' + ff'' - f'^2 - Mf' + Gt\theta + Gc\phi - \frac{A}{2}(\eta f'' + 2f' - 2) + 1 = 0 \quad (3.43)$$

Equation 3.41 represents the dimensionless momentum equation, where $Gt = \frac{g\beta_t T_0}{b^2}$

is the thermal Grashof number; $Gc = \frac{g\beta_c C_0}{b^2}$ is the solutal Grashof number;

$M = \frac{\sigma B_0^2}{\rho b}$ is the magnetic field parameter and $A = \frac{c}{b}$ is the unsteadiness parameter.

3.5.3 Dimensionless Energy Equation

The fluid temperature can be expressed as:

$$T = \frac{T_o x}{(1-ct)^2} \theta + T_\infty \quad (3.44)$$



The radiative heat flux term in the energy equation (3.13) is analysed by using the Rosseland diffusion approximation (Sparrow and Cess, 1961) for an optically thick boundary layer as follows:

$$q_r = -\frac{4\sigma^*}{3K'} \frac{\partial T^4}{\partial y} \quad (3.45)$$

Where K' and σ^* are the mean absorption coefficient and the Stefan-Boltzmann constant respectively. This approximation is valid at points optically far from the bounding surface, and it is good only for intensive absorption, that is, for an optically thick boundary layer (Hossain et al., 2001).

We assume that the temperature differences within the flow such as the term T^4 may be expressed as a linear function of temperature. Hence, expanding T^4 in a Taylor series about T_∞ and neglecting higher order terms, we get;

$$T^4 \cong 4T_\infty^3 T - 3T_\infty^4 \quad (3.46)$$

The first derivative of this with respect y is,

$$\frac{\partial T^4}{\partial y} \cong 4T_\infty^3 \frac{\partial T}{\partial y} \quad (3.47)$$

This simplifies (3.45) to:

$$q_r = -\frac{4\sigma^*}{3K'} * 4T_\infty^3 \frac{\partial T}{\partial y} \quad (3.48)$$

Differentiating with respect to y gives,



$$\frac{\partial q_r}{\partial y} = -\frac{4\sigma^*}{3K'} * 4T_\infty^3 \frac{\partial^2 T}{\partial y^2} \quad (3.49)$$

Thus, substituting all related terms in to the energy equation gives:

$$\begin{aligned} 2T_o c x (1-ct)^{-3} \theta + \frac{1}{2} T_o x y \theta' \sqrt{\frac{b}{v}} c (1-ct)^{-\frac{7}{2}} + \frac{bx}{(1-ct)} f' \cdot \frac{T_o}{(1-ct)^2} \theta + \\ - \sqrt{\frac{bv}{(1-ct)}} f \cdot \frac{T_o x}{(1-ct)^2} \cdot \sqrt{\frac{b}{v(1-ct)}} \theta' = \alpha \frac{T_o bx}{v(1-ct)^3} \theta'' + \frac{v}{c_p} \left(x \sqrt{\frac{b^3}{v(1-ct)^3}} f'' \right)^2 + (3.50) \\ - \frac{\alpha}{\kappa} \left(-\frac{4}{3} Ra \frac{\kappa T_o x b}{(1-ct)^3 v} \theta'' \right) + \frac{\sigma B_o^2}{\rho c_p (1-ct)} \left(\frac{bx}{(1-ct)} f' \right)^2 \end{aligned}$$

Expanding, simplifying and re-arranging yield

$$\left(1 + \frac{4}{3} Ra \right) \theta'' + \text{Pr} (f \theta' - f' \theta) - \frac{A}{2} \text{Pr} (\eta \theta' + 4\theta) + Br (M f'^2 + f''^2) = 0. \quad (3.51)$$

Equation 3.49 is the dimensionless thermal boundary layer equation where $\text{Pr} = \frac{\nu}{\alpha}$ is

the Prandtl number, $Ra = \frac{4\sigma^* T_\infty^3}{\kappa K'}$ is the thermal radiation parameter, and

$Br = \frac{\mu U_\infty^2}{\kappa (T_w - T_\infty)}$ is the Brinkmann number.



3.5.4 Dimensionless Concentration Equation

The species concentration in the fluid is expressed as:

$$C = (C_s - C_\infty) \phi(\eta) + C_\infty \quad (3.52)$$

The partial derivative of C with respect to x and y yields,

$$\frac{\partial C}{\partial x} = -\frac{1}{2} x^{-3/2} y \sqrt{\frac{U_{\infty}}{\nu}} (C_s - C_{\infty}) \phi'(\eta) \quad (3.53)$$

$$\frac{\partial C}{\partial y} = x^{-1/2} \sqrt{\frac{U_{\infty}}{\nu}} (C_s - C_{\infty}) \phi'(\eta) \quad (3.54)$$

$$\frac{\partial^2 C}{\partial y^2} = \frac{U_{\infty} x^{-1}}{\nu} (C_s - C_{\infty}) \phi''(\eta) \quad (3.55)$$

Substituting into the concentration equation gives:

$$\begin{aligned} & U_{\infty} f'(\eta) \left(-\frac{1}{2} x^{-3/2} y \sqrt{\frac{U_{\infty}}{\nu}} (C_s - C_{\infty}) \phi'(\eta) \right) + \\ & \left(\frac{1}{2} U_{\infty} x^{-1} y f'(\eta) - \frac{1}{2} x^{-1/2} \sqrt{\nu U_{\infty}} f(\eta) \right) \cdot x^{-1/2} \sqrt{\frac{U_{\infty}}{\nu}} (C_s - C_{\infty}) \phi'(\eta) = (3.56) \\ & D * \frac{U_{\infty} x^{-1}}{\nu} (C_s - C_{\infty}) \phi''(\eta) - \gamma (C_s - C_{\infty}) \phi(\eta) \end{aligned}$$

Expanding, simplifying and rearranging yield,

$$\phi'' + Sc(f\phi' - f'\phi) - \frac{A}{2} Sc(\eta\phi' + 4\phi) - \beta Sc\phi = 0. \quad (3.57)$$

Equation 3.57 is the dimensionless species concentration boundary layer equation

where $Sc = \frac{\nu}{D}$ is the Schmidt number and $\beta = \frac{\gamma}{b}(1 - ct)$ is reaction rate parameter.



3.5.5 Dimensionless Boundary Conditions

The corresponding boundary conditions are now:

$$f(0) = 0, \quad f'(0) = \varepsilon + \delta f''(0), \quad \theta(0) = 1 + \varsigma \theta', \quad \phi(0) = 1 + \xi \phi',$$

$$f'(\infty)=1, \quad \theta(\infty)=0, \quad \phi(\infty)=0. \quad (3.58)$$

www.udsspace.uds.edu.gh

In the above equations, primes denote the order of differentiation with respect to the similarity variable. Here $\varepsilon = \frac{a}{b}$ is the velocity ratio parameter, $\delta = l\sqrt{b\nu}$ is the dimensionless velocity slip parameter, $\lambda = m\sqrt{\frac{b}{\nu}}$ is the dimensionless thermal slip parameter, $\xi = n\sqrt{\frac{b}{\nu}}$ is the dimensionless solutal slip parameter.

1.6 Dimensionless Fluxes

3.6.1 The Skin Friction Coefficient

The fact that the function $f(\eta)$ gives all information about the flow in the boundary layer must be emphasized. The shear stress can be obtained from it, using Newton's law of viscous shear:

$$\tau_s = \mu \frac{\partial u}{\partial y} \Big|_{y=0} = \mu \frac{\partial}{\partial y} (u_\infty f') \Big|_{y=0} = \mu u_\infty \left(\frac{\partial f'}{\partial \eta} \frac{\partial \eta}{\partial y} \right) \Big|_{y=0} \quad (3.59)$$

From (3.36) we can rewrite (3.59) as,

$$\tau_s = \mu u_\infty \frac{\sqrt{u_\infty}}{\sqrt{\nu x}} \frac{\partial^2 f}{\partial \eta^2} \Big|_{\eta=0} \quad (3.60)$$

We rewrite (3.60) as:

$$\tau_s = \mu u_\infty \frac{\sqrt{u_\infty}}{\sqrt{\nu x}} f''(0) \quad (3.61)$$



The local skin friction coefficient or local skin drag coefficient is defined as,

$$C_f = \frac{2\tau_s}{\rho u_\infty^2} \quad (3.62)$$

Substituting Equation (3.61) into (3.62) we get,

$$C_f = \frac{2\mu u_\infty}{\rho u_\infty^2} \frac{\sqrt{u_\infty}}{\sqrt{\nu x}} f''(0) = \frac{2\nu}{u_\infty} \frac{\sqrt{u_\infty}}{\sqrt{\nu x}} f''(0) \quad (3.63)$$

We simplify to get,

$$C_f = 2 \sqrt{\frac{\nu}{u_\infty x}} f''(0) = 2 \text{Re}_x^{-1/2} f''(0) \quad (3.64)$$

The constant in (3.64) is adjusted to get the local skin friction as,

$$\text{Re}_x^{1/2} C_f = f''(0) \quad (3.65)$$

3.6.2. The Rate of Heat Transfer Coefficient

The rate of conduction of heat transfer coefficients are usually expressed in terms of the Nusselt number:

$$Nu = \frac{x q_s}{\kappa(T_s - T_\infty)}, \quad (3.66)$$

Where q_s is the heat flux at the surface of the plate. In the context of our problem, we define it to be the sum of the convective heat flux and radiative heat flux:



$$q_s = -\kappa \frac{\partial T}{\partial y} \Big|_{y=0} - \frac{4\sigma^*}{3K'} \frac{\partial T^4}{\partial y} \Big|_{y=0} \quad (3.67)$$

Simplifying

$$q_s = -\kappa \frac{\partial T}{\partial y} \Big|_{y=0} - \frac{4\sigma^*}{3K'} \cdot 4T_\infty^3 \frac{\partial T}{\partial y} \Big|_{y=0} \quad (3.68)$$

By factorization, (3.68) becomes,

$$q_s = -\kappa \frac{\partial T}{\partial y} \Big|_{y=0} \left(1 + \frac{4\sigma^* T_\infty^3}{\kappa K'} \cdot \frac{4}{3} \right) \quad (3.69)$$

Further substitution gives

$$q_s = -\kappa x^{-1/2} \sqrt{\frac{U_\infty}{\nu}} (T_s - T_\infty) \theta'(0) \left(1 + \frac{4\sigma^* T_\infty^3}{\kappa K'} \cdot \frac{4}{3} \right) \quad (3.70)$$

We rearrange to get,

$$q_s = -\kappa x^{-1} \sqrt{\frac{U_\infty x}{\nu}} (T_s - T_\infty) \theta'(0) \left(1 + \frac{4\sigma^* T_\infty^3}{\kappa K'} \cdot \frac{4}{3} \right) \quad (3.71)$$

Simplifying gives,

$$q_s = -\text{Re}_x^{1/2} \kappa x^{-1} (T_s - T_\infty) \theta'(0) \left(1 + \frac{4}{3} Ra \right) \quad (3.72)$$

Resulting in



$$Nu = \frac{-x \cdot \kappa x^{-1} \cdot \text{Re}_x^{1/2} (T_s - T_\infty) \cdot \theta'(0) \cdot \left(1 + \frac{4}{3} Ra\right)}{\kappa (T_s - T_\infty)} \quad (3.73)$$

Or

$$Nu = -\text{Re}_x^{1/2} \cdot \left(1 + \frac{4}{3} Ra\right) \cdot \theta'(0) \quad (3.74)$$

Rearranging (3.74) gives,

$$\text{Re}_x^{-1/2} Nu = -\left(1 + \frac{4}{3} Ra\right) \theta'(0) \quad (3.75)$$

3.6.3 The Rate of Mass Transfer Coefficient

The coefficient of mass transfer is generally specified by the Sherwood number:

$$Sh = \frac{x q_m}{D(C_s - C_\infty)} \quad (3.76)$$

Where q_m is the mass diffusion flux.

In the context of this problem, the Fick's law is defined as:

$$q_m = -D \frac{\partial C}{\partial y} \quad (3.77)$$

Substituting terms



$$q_m = -Dx^{-1/2} \sqrt{\frac{U_\infty}{\nu}} (C_s - C_\infty) \phi'(0) \quad (3.78)$$

We simplify (3.78) to get,

$$q_m = -Dx^{-1} \cdot \text{Re}_x^{1/2} (C_s - C_\infty) \phi'(0) \quad (3.79)$$

On further substitutions, we get;

$$Sh = \frac{-x \cdot Dx^{-1} \cdot \text{Re}_x^{1/2} (C_s - C_\infty) \phi'(0)}{D(C_s - C_\infty)} \quad (3.80)$$

We simplify (3.80) to get,

$$Sh = -\text{Re}_x^{1/2} \phi'(0) \quad (3.81)$$

We rearrange (3.81) as

$$\text{Re}_x^{-1/2} Sh = -\phi'(0) \quad (3.83)$$



RESULTS AND DISCUSSIONS

This chapter explores various findings obtained through the mathematical analysis of the dimensionless coupled governing equations in Chapter Three and the associated boundary conditions.

4.1 Numerical Procedure

The non-linear ordinary differential equations are solved with the aid of the fourth-order Runge-Kutta integration algorithm alongside the Newton-Raphson techniques. We begin with some initial guess value and solve the problem with some particular set of parameters to obtain $f''(0)$, $\theta'(0)$ and $\phi'(0)$. The solution process is repeated with another larger value of η_∞ until two successive values of $f''(0)$, $\theta'(0)$ and $\phi'(0)$ differ only after desired digit signifying the limit of the boundary along η . The last value of η_∞ is chosen as appropriate value for that particular simultaneous equation of first order for seven unknowns following the method of superposition.

To solve the system of equations 3.43, 3.51 and 3.57 together with the boundary conditions, we require seven initial conditions, whilst we have only two initial conditions $f(0)$ and $f'(0)$ on f ; and one initial condition each on θ and ϕ . This means that there are three initial conditions $f''(0)$, $\theta'(0)$ and $\phi'(0)$ which are not prescribed. Now, we employ numerical shooting technique where these two ending boundary conditions are utilized to produce two unknown initial conditions at $\eta = 0$. In this calculation, the step size $\Delta\eta = 0.001$ was used while obtaining the numerical solution





with $\eta_{\max}=10$ and six-decimal (10^{-6}) accuracy as the criterion for convergence. The numerical procedure was carried out using a Maple 16 software package. A representative set of numerical results are displayed graphically and discussed qualitatively to show some interesting aspects of some pertinent controlling parameters of the flow on the dimensionless axial velocity profiles, temperature profiles, concentration profiles, local skin friction coefficient, rate of heat transfer and the rate of mass transfer.

4.2. Numerical Results

The results of the study were compared to that of Ishaket *al.*, (2006), Pal (2009) and Chen (2014) as in **Table 4.1**. In the absence of chemical species concentration, radiation, viscous dissipation and magnetic field effects, our work reduces to the work reported

Table 4.1: Values of $f''(0)$ and $-\theta'(0)$ for different values of Pr when $\delta = \zeta = \xi = \alpha = 0$ and $G_t = 1$

Pr	Pal (2009)		Chen (2014)		Present Study	
	$f''(0)$	$-\theta'(0)$	$f''(0)$	$-\theta'(0)$	$f''(0)$	$-\theta'(0)$
0.72	0.36449	1.09331	0.36449	1.09311	0.36449	1.09310
6.80	0.18042	3.28957	0.18042	3.28957	0.18042	3.28957
20.0	0.11750	5.62014	0.11750	5.62013	0.11750	5.62013
40.0	0.08724	7.93831	0.08724	7.93830	0.08724	7.93831
60.0	0.07284	9.71801	0.07284	9.71800	0.07284	9.71801
80.0	0.06394	11.21875	0.06394	11.21873	0.06394	11.21874
100.0	0.05773	12.54113	0.05773	12.54109	0.05773	12.54110

by Chen (2014); and in the absence of chemical species concentration, radiation, viscous dissipation, velocity slip, thermal slip, solutal slip, velocity ratio and magnetic

field effects, our work reduces to that of Pal (2009). From the comparison, the results were observed to be consistent with published results in literature and thus, validate the accuracy of the numerical procedure.

Table 4.2 shows the numerical results of skin friction coefficient, local Nusselt number (Heat transfer rate) and the local Sherwood number (Mass transfer rate) with varying values of the Prandtl number (Pr), magnetic parameter (M), reaction rate parameter (β), radiation parameter (Ra), Brinkmann number (Br) and Schmidt number (Sc). It was observed that the skin friction increases with increasing values of M , Pr , Sc and β ; and decreases with increasing values of Ra and Br . This means that the effect of Lorentz force, momentum diffusion and chemical reaction is to increase the local skin friction; whereas the combined effect of radiation and viscous dissipation reduce the skin friction at the surface of the plate.

Meanwhile, the rate of heat transfer increases with increasing values of Pr and decreases with increasing values of M , β , Ra , Br and Sc . Moreover, it was observed that increasing values of β , Ra , Br and Sc lead to increasing the rate of mass transfer. This effect can be explained by the presence of chemical reaction, mass diffusion, radiation and viscous dissipation. Also increasing values of Pr and M tend to reduce the rate at which mass is transferred at the surface of the plate.



Table 4.2 Results of skin friction coefficient, Nusselt and Sherwood numbers for various values of Pr , M , β , Ra , Br and Sc

Pr	M	β	Ra	Br	Sc	$f''(0)$	$-\theta'(0)$	$-\phi'(0)$
0.72	0.1	0.1	0.1	0.1	0.24	-0.66020	0.83208	0.57015
4.00						-0.64566	1.71274	0.56882
7.10						-0.56416	2.13843	0.56855
	1.0					-0.25933	0.72248	0.51371
	1.5					-0.09921	0.68058	0.48905
		1.0				-0.65692	0.83162	0.70193
		1.5				-0.65547	0.83142	0.76453
			1.0			-0.66631	0.60923	0.57090
			1.5			-0.66837	0.54546	0.57117
				1.0		-0.66420	0.67815	0.57072
				1.5		-0.66644	0.59136	0.57103
					1.78	-0.64299	0.82978	1.34744
					2.64	-0.63982	0.82944	1.58050

Table 4.3 shows the numerical results of skin friction coefficient, local Nusselt number (Heat transfer rate) and the local Sherwood number (Mass transfer rate) with varying values of thermal Grashof number (Gt), solutal Grashof number (Gc), unsteadiness parameter (A), velocity ratio parameter (ϵ), velocity slip parameter (δ), thermal slip parameter (ζ) and solutal slip parameter (ξ). It was observed that the skin friction increases with increasing values of δ , ζ and ξ ; and decreases with increasing values of Gt , Gc , A , and ϵ . This means that the effect of velocity, thermal and solutal slips at the surface of the sheet is to increase the local skin friction; whereas the combined effect of buoyancy forces (due to thermal and solutal diffusion);



unsteadiness of the flow; and the difference in the velocities upstream and at the surface of the sheet, are to reduce the skin friction at the surface of the sheet. Meanwhile, it was observed that the rate of heat transfer increases with increasing values of Gt , Gc , A , ε and δ ; and decreases with increasing values of ζ and ξ . Furthermore, the rate of mass transfer increases with increasing values of Gt , Gc , A , ε and δ ; and decrease with increasing values of ζ and ξ for obvious reasons.

Table 4.3 Results of skin friction coefficient, Nusselt and Sherwood numbers for various values of Gt , Gc , A , ε , δ , ζ and ξ .

Gt	Gc	A	ε	δ	ζ	ξ	$f''(0)$	$-\theta'(0)$	$-\phi'(0)$
0.1	0.1	0.1	0.5	0.1	0.1	0.1	-0.66020	0.83208	0.57015
1.0							-0.94992	0.85599	0.58810
1.5							-1.10336	0.86708	0.59709
	1.0						-1.01202	0.86340	0.59531
	1.5						-1.19654	0.87717	0.60756
		1.0					-0.73419	1.17504	0.78571
		1.5					-0.77184	1.32111	0.88129
			1.0				-0.00198	0.93723	0.61884
			1.5				-0.75365	1.00868	0.66161
				1.0			-0.30822	0.89471	0.59802
				1.5			-0.23640	0.90556	0.60315
					1.0		-0.64622	0.47131	0.56927
					1.5		-0.64267	0.37991	0.56904
						1.0	-0.64637	0.83069	0.37635
						1.5	-0.64209	0.83026	0.31664



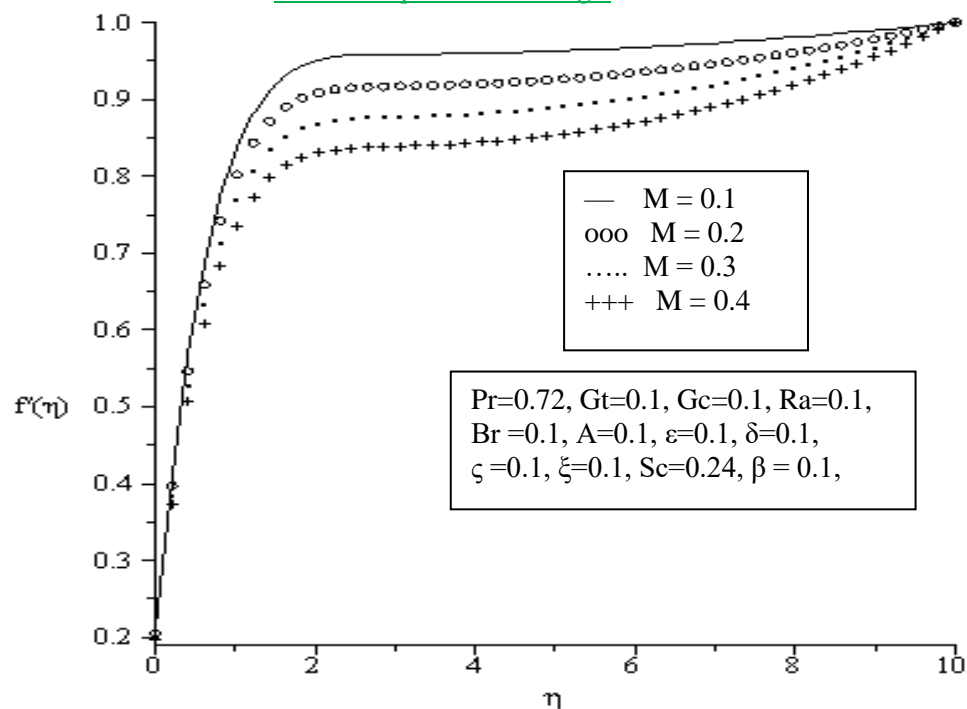
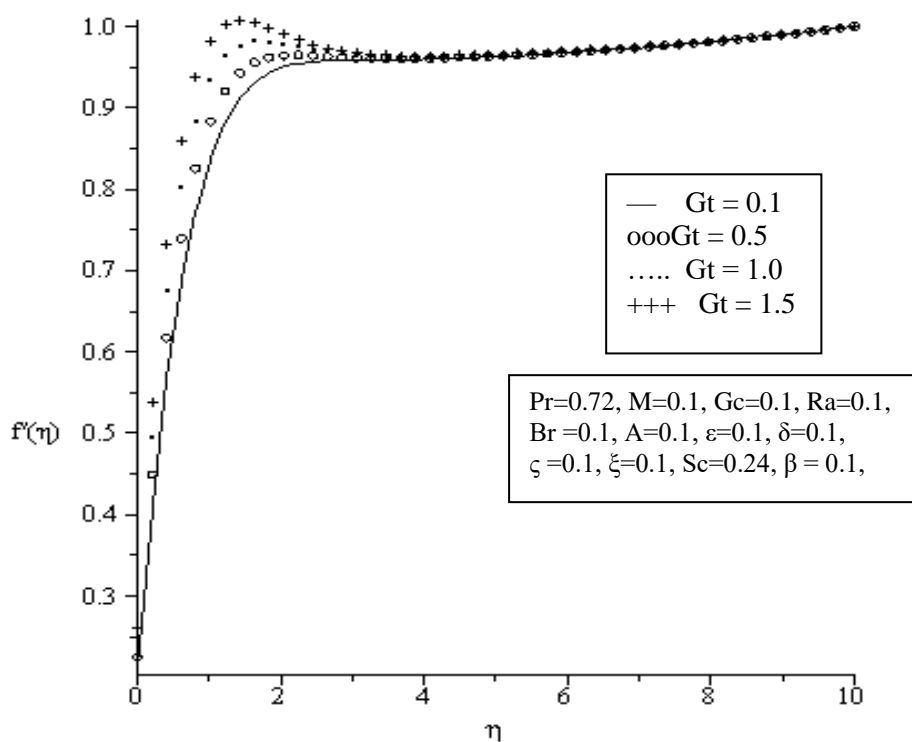
4.3 Graphical Results

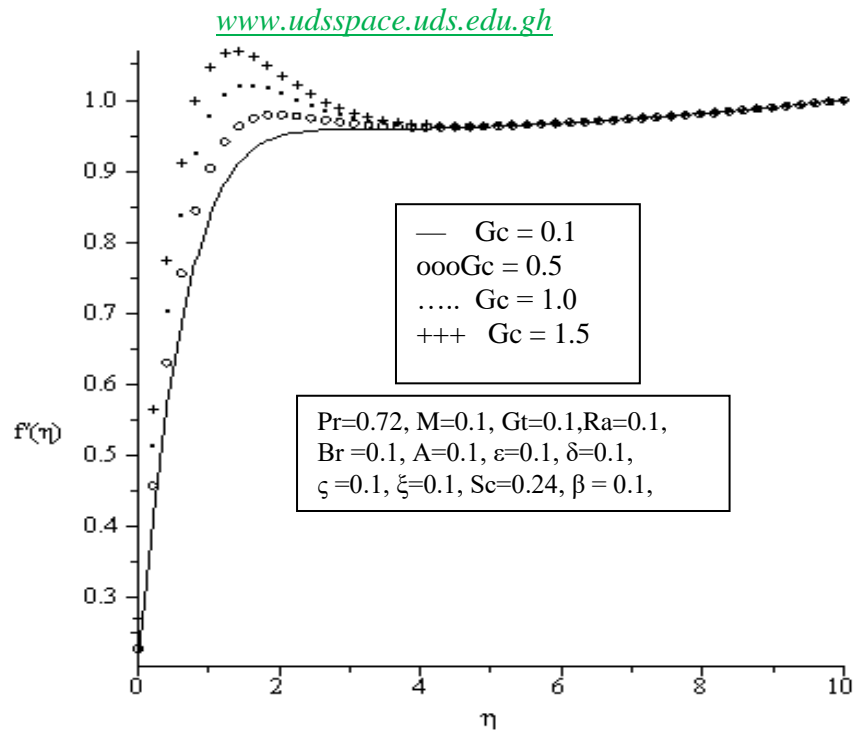
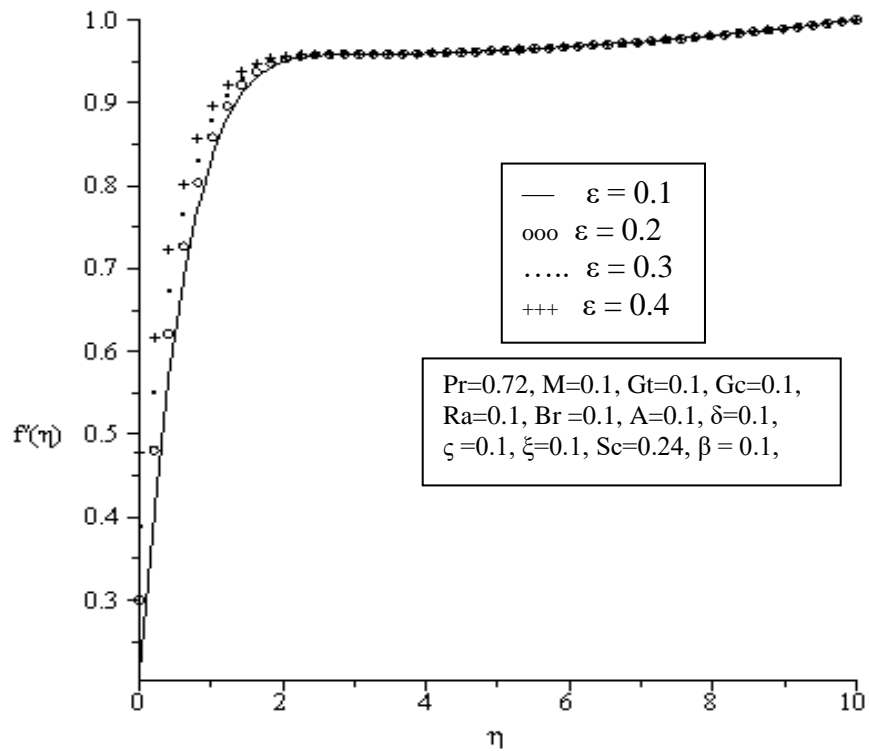
4.3.1. Velocity Profiles

The effect of varying the controlling parameters on the velocity boundary layer is depicted in Figures 4.1-4.5. From Figure 4.1, a consistent decrease in the longitudinal velocity informed by increasing magnetic field intensity (M) with all profiles tending asymptotically to the free stream value away from the plate is observed. In practice, this phenomenon is due to the fact that increasing the magnetic field strength increases the Lorentz force which causes a greater opposition to fluid transport.

It is observed in Figures 4.2 and 4.3 that increasing the thermal and solutal Grashof number (G_t , G_c), respectively lead to increasing the velocity profiles due to induced buoyancy forces. Also from Figures 4.4 and 4.5, increasing the velocity ratio and the unsteadiness parameter tend to increase the thickness of the velocity profile. This is obvious due to the fact that an increase in the velocity ratio means increase in velocity upstream against that on the surface of the sheet causing the thickening of the velocity boundary layer.



Figure 4.1 Velocity profiles for varying values of magnetic parameter (M)Figure 4.2 Velocity profiles for varying values of thermal Grashof number (Gt)

Figure 4.3 Velocity profiles for varying values of SolutalGrashof number (Gc)Figure 4.4 Velocity profiles for varying values of velocity ratio parameter (ε)

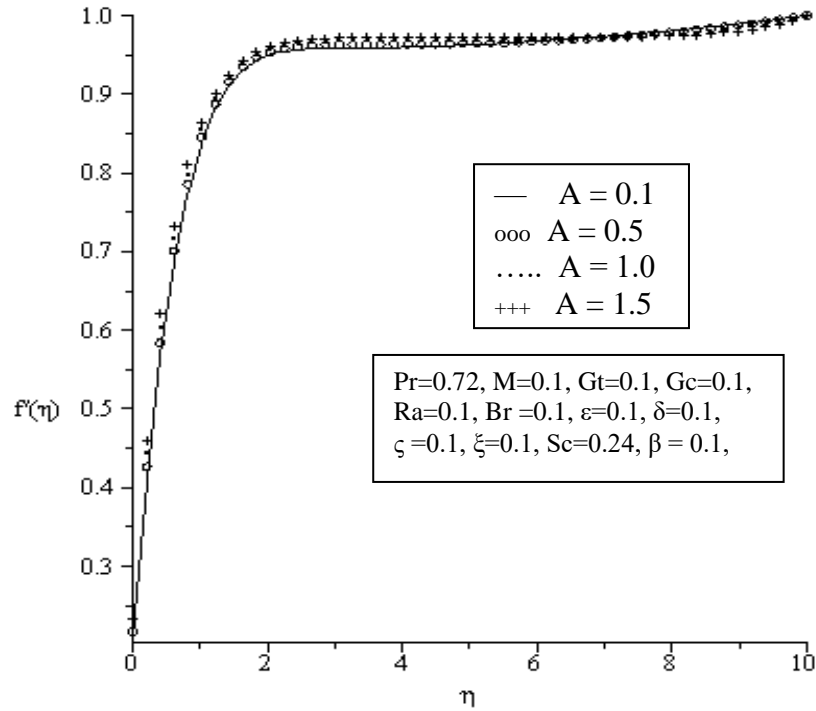


Figure 4.5 Velocity profiles for varying values of unsteadiness parameter (A)

4.3.2. Temperature Profiles

Figures 4.6 – 4.15 show the effects of the Magnetic parameter (M), Prandtl number (Pr), Radiation parameter (Ra), Brinkmann number (Br), thermal Grashof number (Gt), solutalGrashof number (Gc), unsteadiness parameter (A), velocity ratio parameter (ϵ), velocity slip parameter (δ) and thermal slip parameter (ζ) respectively on the temperature profiles. It is observed that increasing the magnetic field intensity increases the fluid temperature which in turn, increases the thermal boundary layer (Figure 4.6). This can be attributed to the effect of Ohmic heating on the flow system.

Meanwhile, increasing Pr decreases the fluid temperature within the boundary layer (Figure 4.7). When Pr is high, the fluid velocity decreases, which implies lower





thermal diffusivity and hence, decrease in fluid temperature. Increasing the Ra causes an increase in the fluid temperature within the boundary layer which in turn, increases the thermal boundary layer (Figure 4.8). In Figure 4.9, it was observed that the same trend occurs for the Brinkmann number due to viscous dissipation.

Moreover, an increase in Gt and Gc as depicted in Figures 4.10 and 4.11 shows a corresponding decrease in the thermal boundary layer as a result of the induced buoyancy forces. Conversely, increasing values of A tend to shrink the thermal boundary layer due to the unsteadiness of the flow (Figure 4.12).

Lastly, in Figures 4.13, 4.14, and 4.15, it was observed that increasing values of ε , δ and ς tend to increase the thermal boundary layer. This means that the combined effects of the differences in velocity upstream and on the surface of the sheet (ε), fluid slip due to velocity of the flow (δ) and fluid slip associated with thermal distribution of the flow (ς) are to decrease the temperature of the flow.

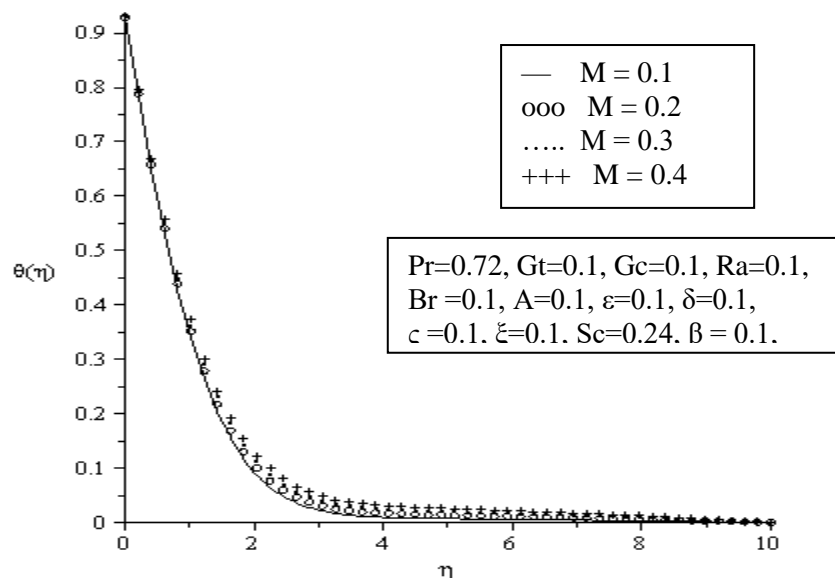


Figure 4.6 Temperature profiles for varying values of Magnetic parameter (M)

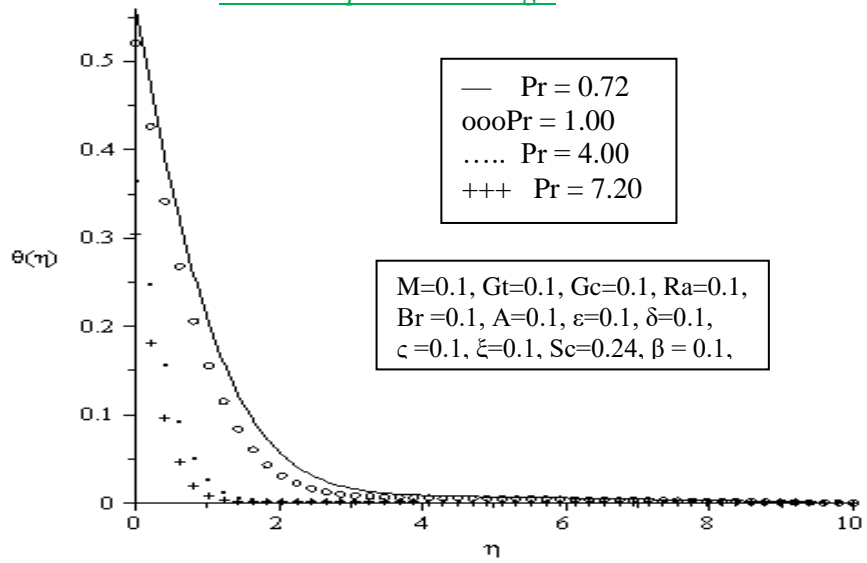


Figure 4.7 Temperature profiles for varying values of Prandtl number (Pr)

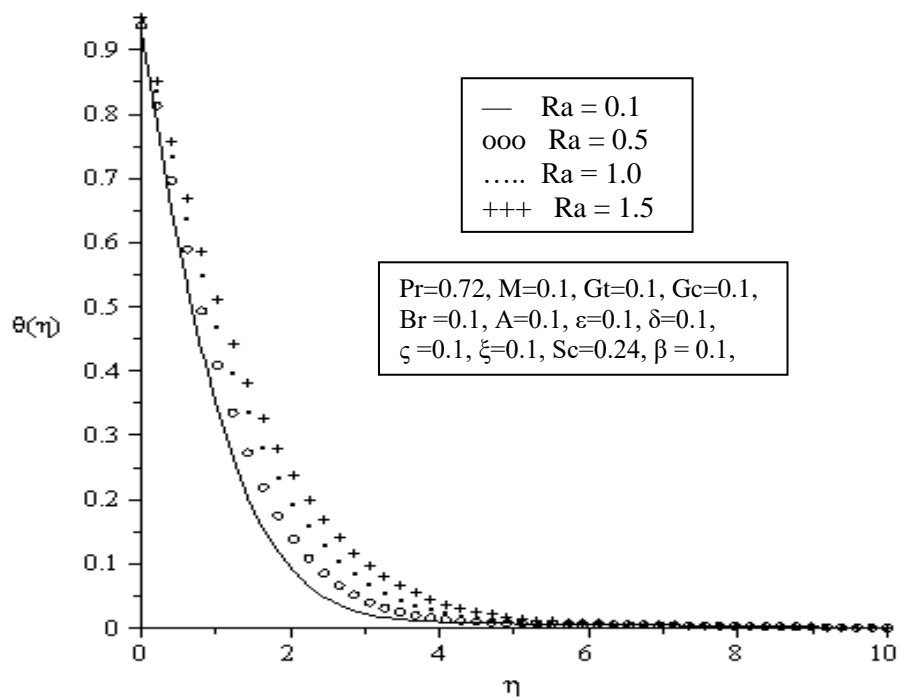


Figure 4.8 Temperature profiles for varying values of radiation parameter (Ra)



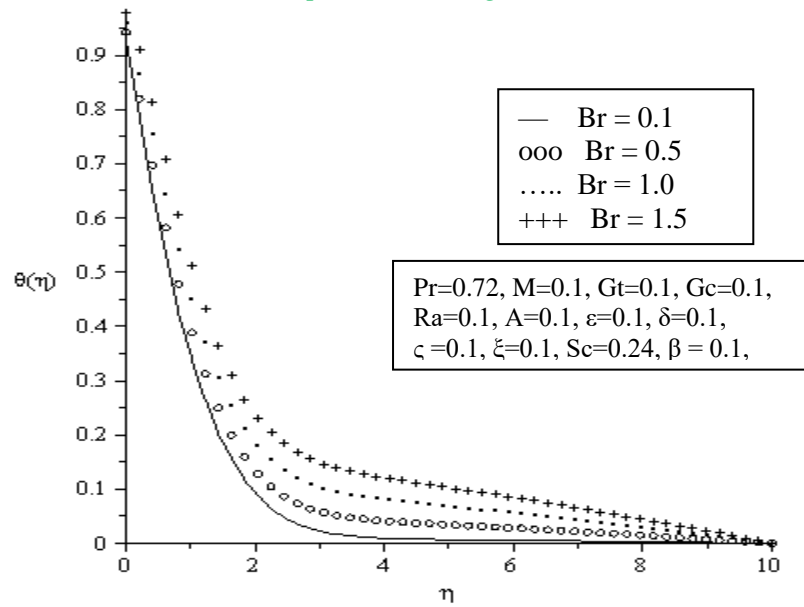


Figure 4.9 Temperature profiles for varying values of Brinkmann number (Br)

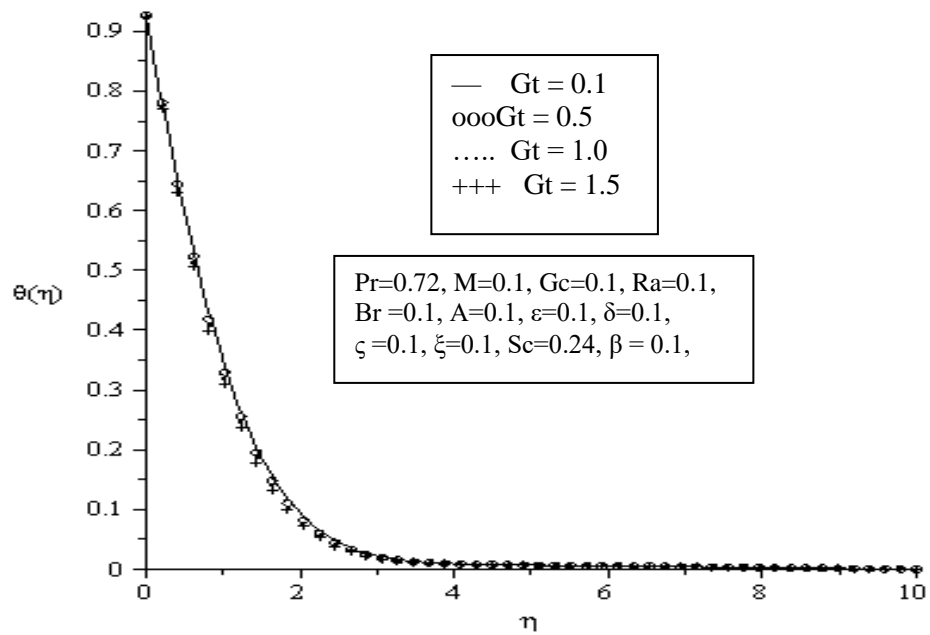


Figure 4.10 Temperature profiles for varying thermal Grashof number (Gt)



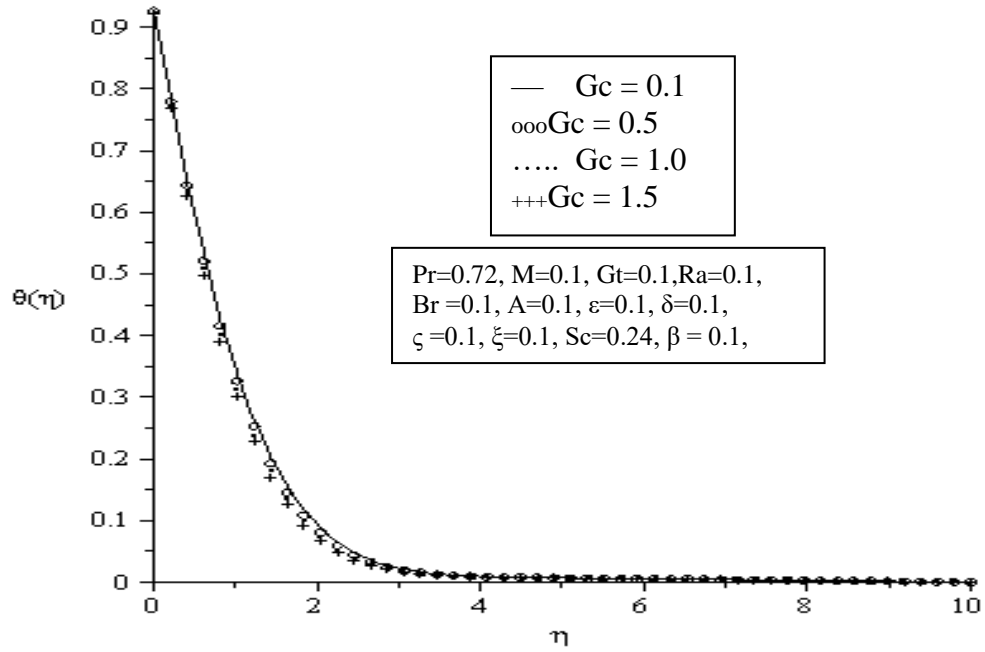


Figure 4.11 Temperature profiles for varying solutal Grashof number (Gc)

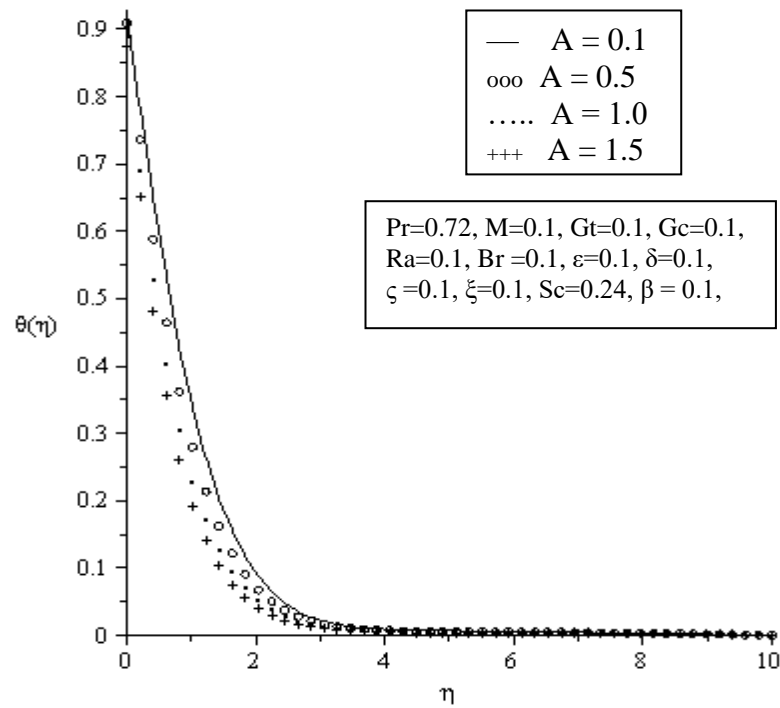


Figure 4.12 Temperature profiles for varying values of unsteadiness Parameter (A)



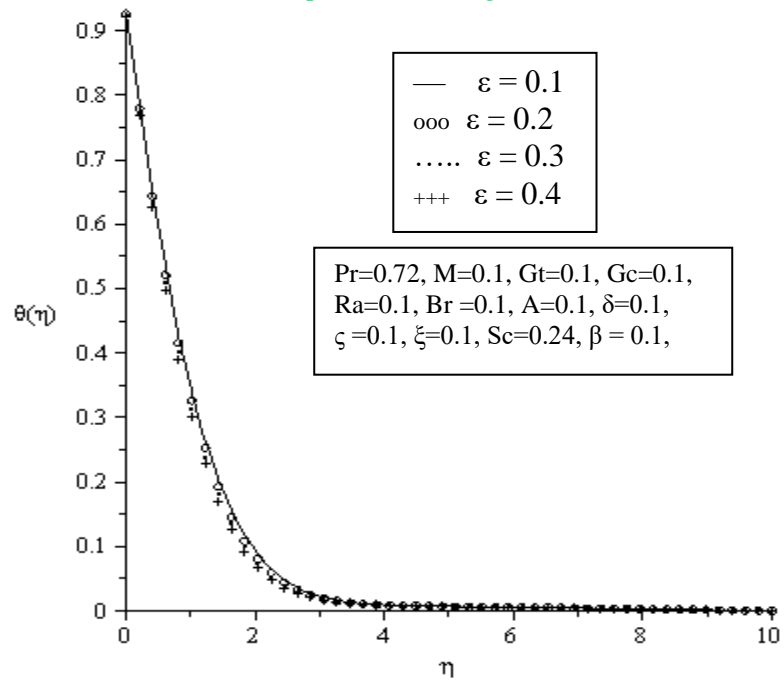


Figure 4.13 Temperature profiles for varying values of Velocity Ratio Parameter (ϵ)

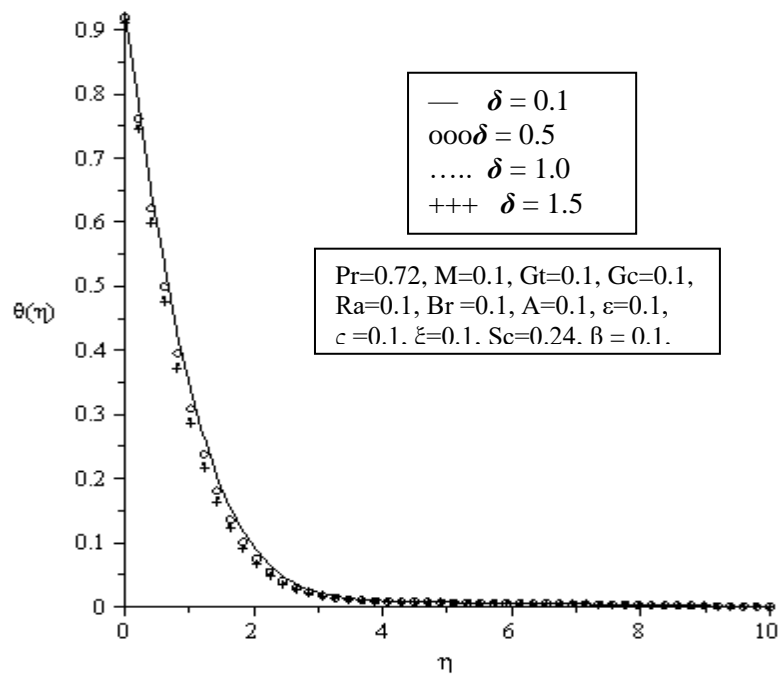


Figure 4.14 Temperature profiles for varying values of Velocity slip Parameter (δ)



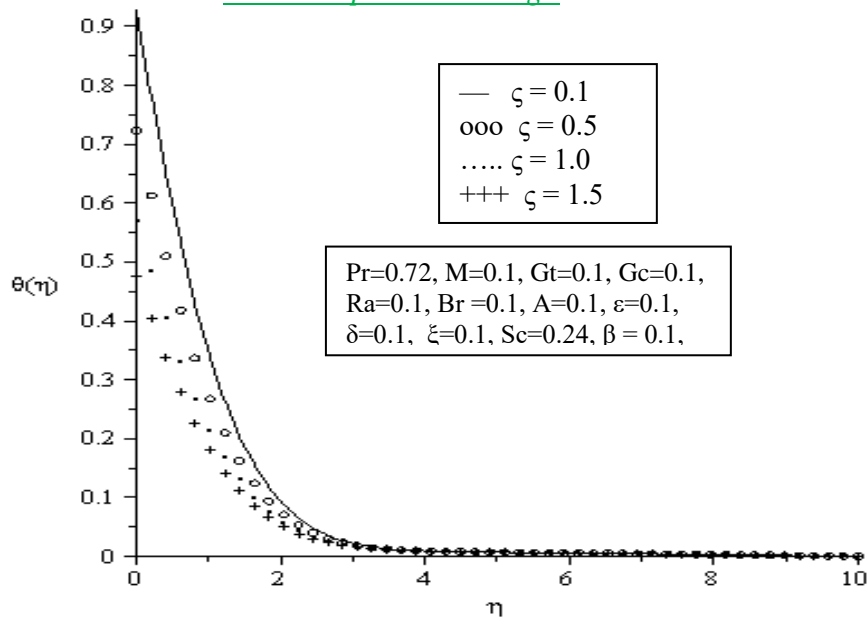


Figure 4.15 Temperature profiles for varying values of thermal slip Ratio Parameter
(ζ)

4.3.3 Concentration Profiles

Figures 4.16 – 4.24 show the effects of the Magnetic field parameter (M), reaction rate parameter (β), Schmidt number (Sc), thermal Grashof number (Gt), solutal Grashof number (Gc), unsteadiness parameter (A), velocity ratio parameter (ϵ), velocity slip parameter (δ) and solutal slip parameter (ξ) respectively on the concentration boundary layer. It is observed that increasing values of M increases the species concentration boundary layer thickness (Figure 4.16). The opposite is true for increasing reaction rate parameter (Figure 4.17) and the Schmidt number (Figure 4.18) since increasing the Schmidt number in particular implies momentum diffusivity dominates mass species diffusivity. Though increasing the reaction rate parameter implies increasing rate of reaction over momentum, it is interesting to note that, the concentration boundary layer reduces. This can be due to the fact that the

reaction rate in this study is destructive and hence has adverse effect on the concentration boundary layer thickness.

From Figures 4.19 and 4.20, the buoyancy forces induced by the increasing values G_t and G_c tend to reduce the concentration boundary layer thickness. Likewise, from Figures 4.21-4.24, the combined effects of A , ε , δ and ξ are to shrink the concentration boundary layer thickness.

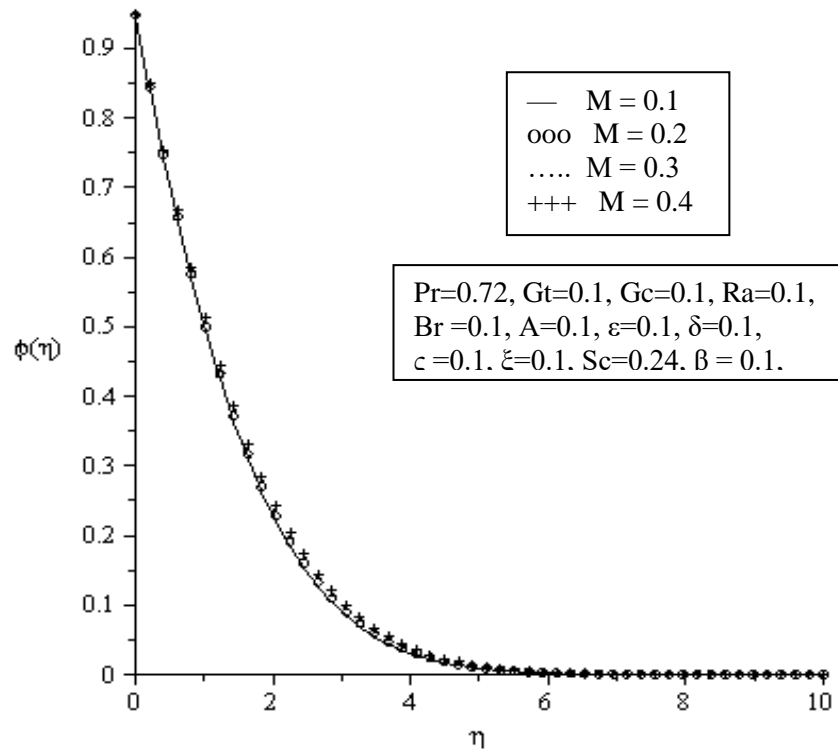


Figure 4.16 Concentration profiles for varying values of magnetic parameter (M)

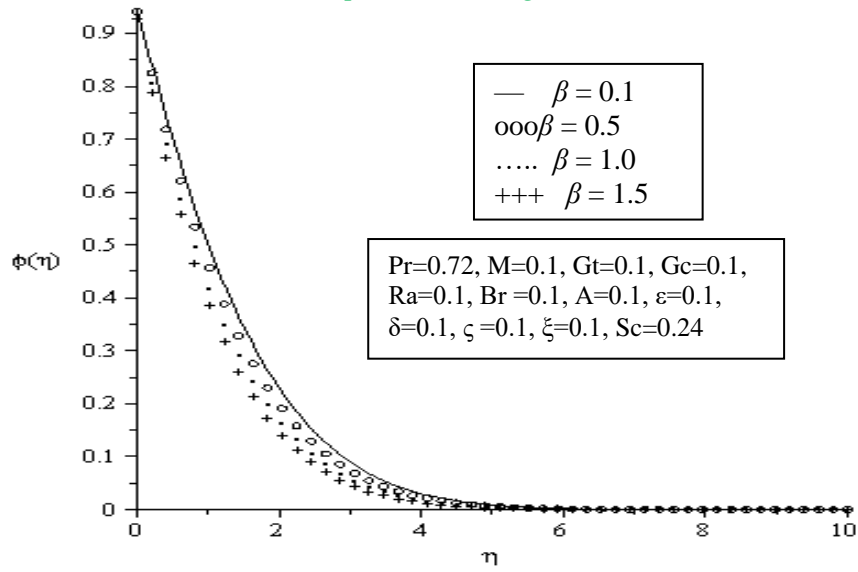


Figure 4.17 Concentration profiles for varying values of reaction rate parameter (β)

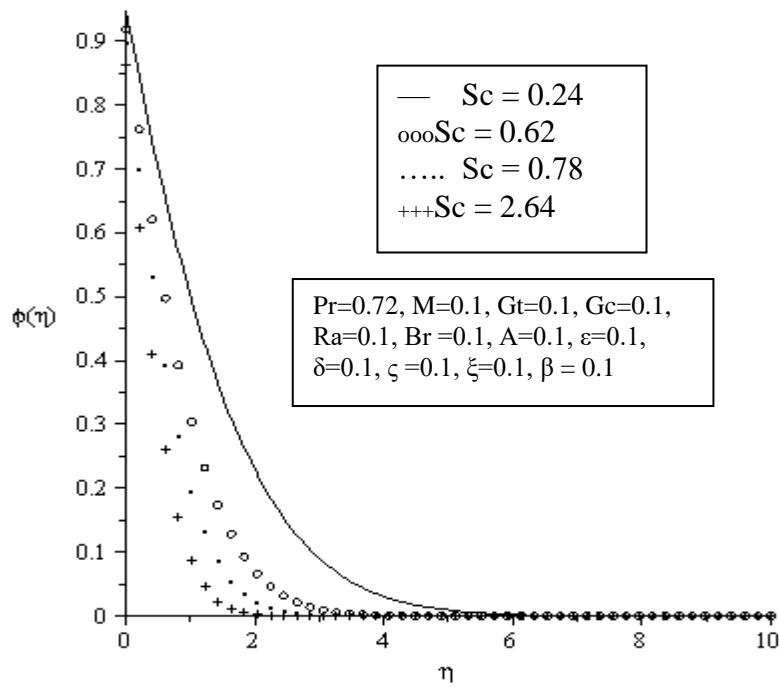


Figure 4.18 Concentration profiles for varying values of Schmidt number (Sc)



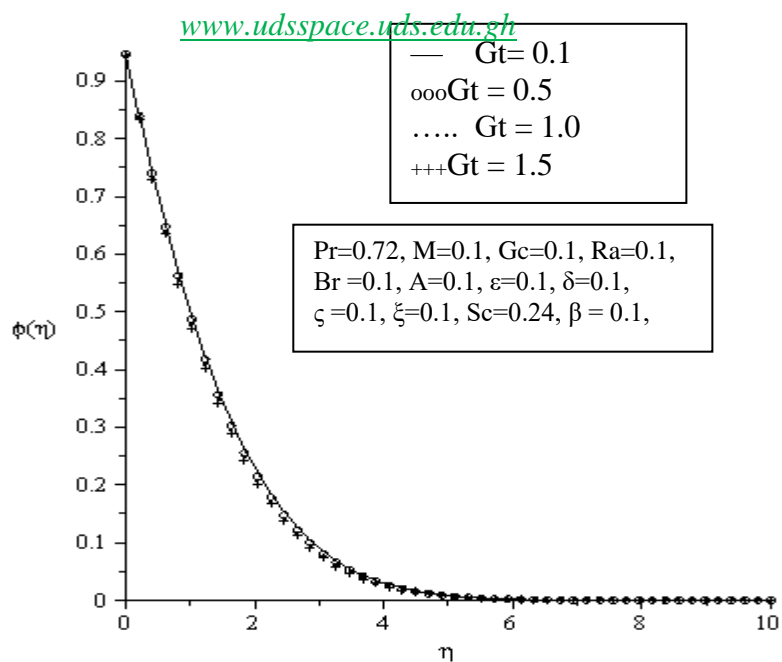


Figure 4.19 Concentration profiles for varying values of thermal Grashof number

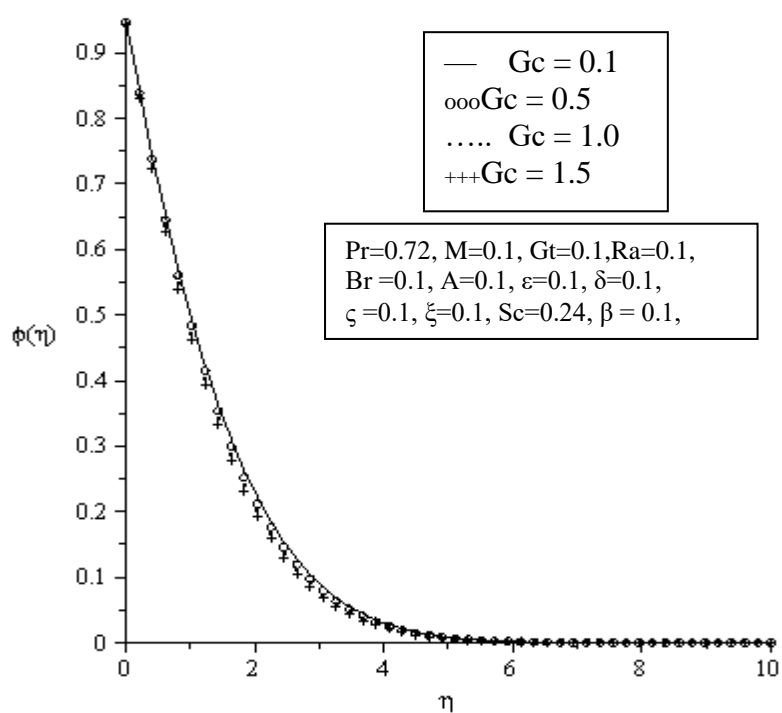


Figure 4.20 Concentration profiles for varying values of Solutal Grashof number

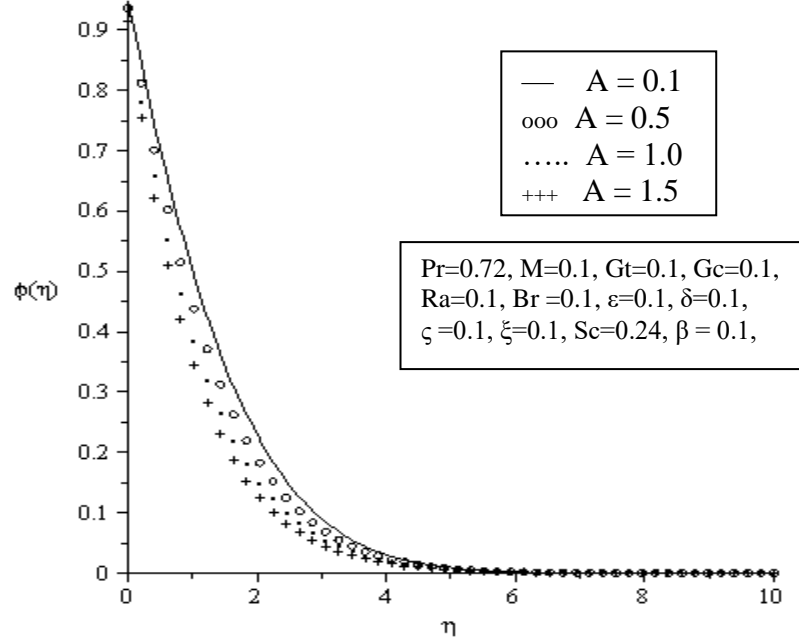


Figure 4.21 Concentration profiles for varying values of unsteadiness parameter (A)

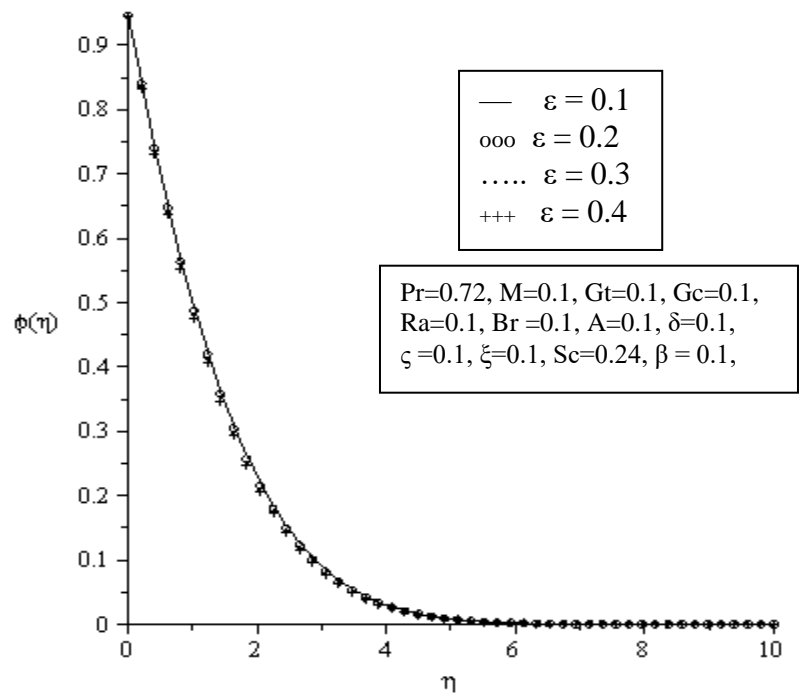


Figure 4.22 Concentration profiles for varying values of velocity ratio parameter (ϵ)



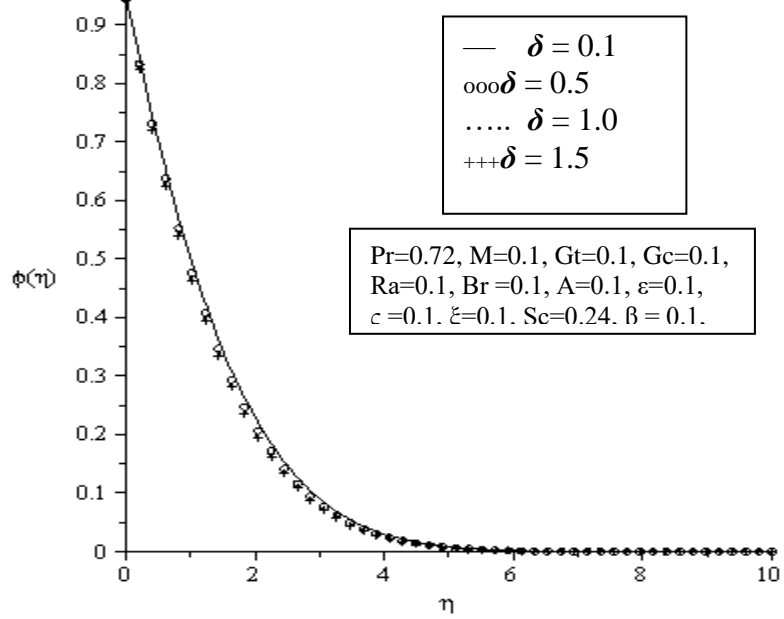


Figure 4.23 Concentration profiles for varying values of velocity slip parameter (δ)

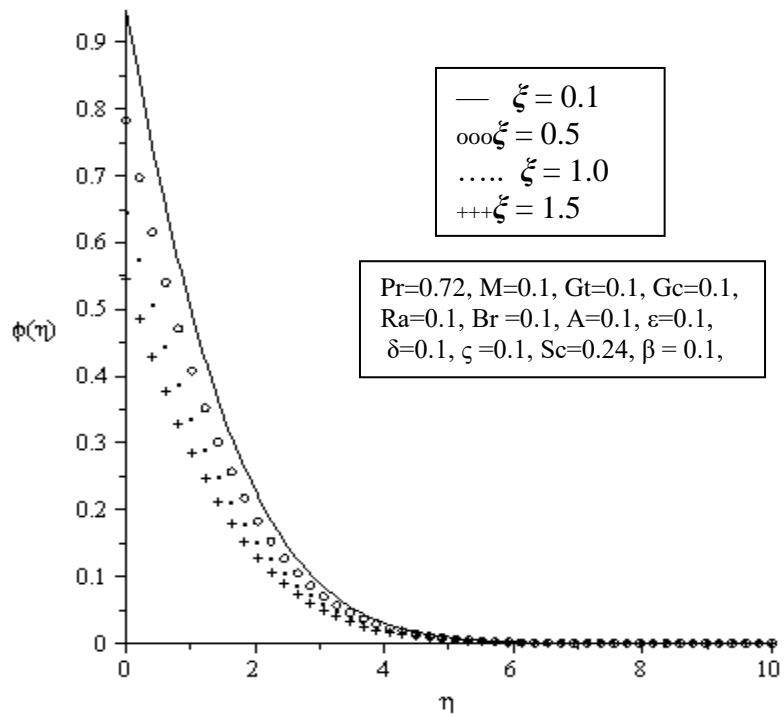


Figure 4.24 Concentration profiles for varying values of solutal slip parameter (ξ)



The behaviour of the convection unsteady stagnation-point flow towards a stretching sheet with slip has been studied. The skin friction increases with increasing M , Pr , δ , ς , ξ , Sc , and β ; and decreases with increasing Gt , Gc , A , ϵ , Ra and Br . The rate of heat transfer increases with increasing Pr , Gt , Gc , A , ϵ , δ and decreases with increasing M , β , Ra , Br , Sc , ς and ξ . Increasing the values of Gt , Gc , A , ϵ , δ , β , Ra , Br and Sc increases the rate of mass transfer; whereas increasing the values of Pr , M , ς and ξ reduces it. The velocity profile increases with increasing Gt , Gc , A and ϵ ; and decreases with increasing M . The temperature profile increases with increasing Ra and Br ; and decreases with increasing Gt , Gc , A , ϵ , δ , and ξ . The concentration profile increases with increasing M ; and decreases with increasing Gt , Gc , A , ϵ , δ , β , Sc and ξ .



CHAPTER FIVE

CONCLUSIONS AND RECOMMENDATIONS

An investigation into the combined effects of partial slip at the stagnation point of an unsteady hydro magnetic flow over a vertical stretching sheet has been investigated. The equations governing the flow were modelled with their associated boundary conditions. To make the resulting coupled partial differential equations solvable numerically, similarity analysis was employed which reduced the problem to a set of nonlinear ordinary differential equations. The nonlinear ordinary differential equations 3.43, 3.51 and 3.57 together with the boundary conditions were then solved by the Runge-Kutta integration method along with the Newton Raphson Algorithm using Maple 16 software.

5.1. Conclusion

Heat and mass transfer in unsteady hydro-magnetic fluid flow over a vertical surface with stagnation point in the presence of radiation and viscous dissipation has been studied. The results of the study were compared to those of Ishaket *al.*, (2006), Pal (2009) and Chen (2014) and they were consistent with them.

The main conclusions from this research is that buoyancy forces, radiation effects, viscous dissipation, partial slip effects, chemical reaction, mass diffusion, momentum diffusion and magnetic fields, highly influence the following parameters:

- i. Fluid velocity;
- ii. Skin friction coefficient;
- iii. The rate of heat and mass transfer; and
- iv. The thickness of both the thermal and concentration boundary layers in unsteady hydro-magnetic fluid flow over vertical surfaces



5.2. Recommendations

The following recommendations are made:

- i. Partial slip study should be extended to include non-Newtonian fluids as they are the most common industrial fluids.
- ii. Future research should consider surfaces with varying orientation
- iii. Research in circular conduits under partial slip and unsteady flow as occur in start-up processes could be very relevant to process industries.



REFERENCES

Abdelkhalek, M. M. (2009). Heat and Mass transfer in MHD free convection from a moving permeable vertical surface by a perturbation technique.

Communication Nonlinear Science Numerical Simulation, 14(5): 2091-2102

Aman, F., Ishak, A. and I. Pop, (2011). Mixed convection boundary layer flow near stagnation-point on vertical surface with slip, *Applied Mathematics and Mechanics*, 32(12), 1599–1606.

Andersson, H. I. (2002). Slip flow past a stretching surface, *Acta Mechanica*, 158 (1-2), 121–125.

Ariel, P. D. (2008). Two dimensional stagnation point flow of an elastico-viscous fluid with partial slip, *Zeitschrift für Angewandte Mathematik und Mechanik*, 88(4), 320–324.

Arthur, E. M. and Seini, Y. I. (2014). Hydromagnetic stagnation point flow over a porous stretching surface in the presence of radiation and viscous dissipation. *Applied and Computational Mathematics*, 3(5), 191-196. doi: 10.11648/j.acm.20140305.11

Aurang Z, Bhattacharyya, K., Shafie, S. (2016) Effect of partial slip on an unsteady MHD mixed convection stagnation-point flow of a micropolar fluid towards a permeable shrinking sheet. *Alexandria Engineering Journal*. Volume 55, Issue 2, June 2016, 1285–1293

Aurang Z. (2015) Slip Effect on an Unsteady MHD Stagnation-Point Flow of a Micropolar Fluid towards a Shrinking Sheet with Thermophoresis Effect. *International Journal for Computational Methods in Engineering Science and Mechanics*.

Bachok, N., Ishak, A. and Nazar, R. (2011). Flow and heat transfer over an unsteady stretching sheet in a micropolar fluid, *Meccanica*, 46(5), 935–942.





- Bhattacharyya, K. (2011). www.udsspace.uds.edu.gh Dual solutions in unsteady stagnation-point flow over a shrinking sheet, *Chinese Physics Letters*, 28(8), Article ID 084702
- Bhattacharyya, K., Mukhopadhyay, S. and Layek, G. C. (2011). Slip effects on an unsteady boundary layer stagnation-point flow and heat transfer towards a stretching sheet, *Chinese Physics Letters*, 28(9).
- Bhattacharyya, K., Arif, Md. G. and Ali Pramanik, W. (2012). MHD boundary layer stagnation-point flow and mass transfer over a permeable shrinking sheet with suction/blowing and chemical reaction, *Acta Technica*, 57(1), 1–15.
- Bhattacharyya, K. and Vajravelu, K. (2012). Stagnation-point flow and heat transfer over an exponentially shrinking sheet, *Communications in Nonlinear Science and Numerical Simulation*, 17(7), 2728–2734.
- Bhattacharyya, K., Uddin, M. S. and Layek, G. C. (2013). Effect of partial slip on boundary layer mixed convective flow adjacent to a vertical permeable stretching sheet in porous medium, *Acta Technica*, 58(1), 27–39.
- Çengel, Y. A. and Cimbala, J. M. (2006). *Fluid mechanics: fundamentals and applications* (1 ed.). New York, America: McGraw-Hill.
- Chamkha (2004). Unsteady MHD convective heat and mass transfer past a semi-infinite vertical permeable moving plate with heat absorption.
- Çengel, Y. A., & Cimbala, J. M. (2006). *Fluid Mechanics: Fundamentals and Applications* (2nd ed.). New York: McGraw-Hill. (A fine undergraduate-level fluid mechanics textbook.)



- Chen, H. (2014), Mixed Convection Unsteady Stagnation-Point Flow towards a
www.udsspace.uds.edu.gh
 Stretching Sheet with Slip Effects. *Mathematical Problems in Engineering*,
 Vol. 2014.
- Chiam, T. C. (1994). Stagnation-point flow towards a stretching plate, *Journal of the
 Physical Society of Japan*, 63(6), 2443–2444.
- Cao, K. and Baker, J. (2009). Slip effects on mixed convective flow and heat transfer
 from a vertical plate, *International Journal of Heat and Mass Transfer*, Vol.
 52:3829–3841.
- Devi, C. D. S., Takhar, H. S. and Nath, G. (1991). Unsteady mixed convection flow in
 stagnation region adjacent to a vertical surface, *Wärme- und
 Stoffübertragung*, 26(2), 71–79.
- Fang, T., Zhang, J. and Yao, S. (2009). Slip MHD viscous flow over a stretching
 sheet—an exact solution, *Communications in Nonlinear Science and
 Numerical Simulation*, 14(11), 3731–3737.
- Fauzi, N. F. S. Ahmad and I. Pop (2015) Stagnation point flow and heat transfer over a
 nonlinear shrinking sheet with slip effects. *Alexandria Engineering Journal*
Volume 54, Issue 4, December 2015, Pages 929–934
- Fotini Labropulu, Daiming Li (2016) Unsteady Stagnation-point Flow of a
 Second-grade Fluid *Journal of Fluid Flow, Heat and Mass Transfer*
(JFFHMT) ISSN: 2368 6111.



- Gupta, V. (2008), Heat and Mass Transfer, www.udsspace.uds.edu.gh New Age International Publishers limited, page 1.
- Hayat, T., Qasim, M. and Abbas, Z. (2010). Homotopy solution for the unsteady three-dimensional MHD flow and mass transfer in a porous space, *Communications in Nonlinear Science and Numerical Simulation*, 15(9), 2375–2387.
- Hayat, T., M. Nawaz (2016). MHD stagnation-point flow of an upper-converted Maxwell fluid over a stretching surface. *Fractals Volume, 30 January 2009, Pages 840–848*
- Hayat, T., Shehzad, S. A., Rafique, A. and Malik, M. Y. (2012). Mixed convection unsteady stagnation point flow over a stretching sheet with heat transfer in the presence of variable free stream, *International Journal for Numerical Methods in Fluids*, 68(4), 483–493.
- Hossain, M. A., Khanafer, K., Vafai, K. (2001). The effect of radiation on free convection flow of fluid with variable viscosity from a porous vertical plate. *Int. J. Therm. Sci.*, 40, 115–124.
- Hiemenz, K. (1911). Die Grenzschicht in Einem in Dem Gleichförmigen Flüssigkeitsstrom Eingetauchten Geraden Kreiszylinder, *Dingler's Polytechnic Journal*, vol. 326, 321–410.
- Homann, F. (1936). Die Einflussgrösse Zähigkeit bei der Strömung um den Zylinder und um die Kugel, *Zeitschrift für Angewandte Mathematik und Mechanik*, 16(3), 153–164.



Howarth, L. (1938). www.udsspace.uds.edu.gh
Proceedings of the Royal Society of London, 164(919), 547–579.

<http://www.spectrose.com/modes-of-heat-transfer-conduction-convection-radiation.html>

http://www.engineeringarchives.com/les_fm_noslip.html

<https://riverrestoration.wikispaces.com/hydraulics>

Hui, Chen (2015). Mixed Convection Unsteady Stagnation-Point.
International Journal for Computational Methods in Engineering Science and Mechanics.

Ishak, A., Nazar, R. and Pop, I. (2006). Mixed convection boundary layers in the stagnation-point flow toward a stretching vertical sheet, *Meccanica*, 41(5), 509–518.

Ishak, A., Nazar, R., Bachok, N. and Pop, I. (2010). MHD mixed convection flow near the stagnation-point on a vertical permeable surface, *Physica A: Statistical Mechanics and its Applications*, 389(1), 40–46

Ishak, A., Nazar, R. and Pop, I. (2008). Mixed convection stagnation point flow of a micropolar fluid towards a stretching sheet, *Meccanica*, 43(4), 411–418

- Ishak, A., Nazar, R. and Pop, I. (2009). Heat transfer over an unsteady stretching permeable surface with prescribed wall temperature, *Nonlinear Analysis: Real World Applications*, 10(5), 2909–2913.6
- J. Mitchell (1950). Bessemer converter for making iron and steel, *Journal Iron and Steel Institute.*, 1950, vol. 165, p.5.
- Jean B. J. Fourier (1768 – 1830). In the Academy of science, Paris. *Girandon/Art Resource, New York*
- Kohilavani N., Roslinda N. and Loan P. (2015). Unsteady stagnation point flow and heat transfer of a special third grade fluid past a permeable stretching/shrinking sheet, *a natureresearch journal*.
- Khairy Z. and Anuar I. (2016) Stagnation-Point Flow towards a Stretching Vertical Sheet with Slip Effects
- Khalid.M, Aurang Z. Krishnendu B. Sharidan S. (2016). Multiple Solutions of an Unsteady Stagnation-Point Flow with Melting Heat Transfer in a Darcy–Brinkman Porous Medium. *Nonlinear Engineering, Volume 5, Issue 2, pp 99 - 106*
- Lok, Y. Y., Amin, N. and Pop, I. (2006). Unsteady mixed convection flow of a micropolar fluid near the stagnation point on a vertical surface, *International Journal of Thermal Sciences*, 45(12), 1149–1157.
- Lienhard IV, J. H. and Lienhard V, J. H. (2008). *Heat Transfer Text Book* (3 ed.). Cambridge, USA: Phlogiston Press





www.udsspace.uds.edu.gh
 Layek, G. C., Mukhopadhyay, S. and Samad, S. A. (2007). Heat and mass transfer analysis for boundary layer stagnation point flow towards a heated porous stretching sheet with heat absorption/generation and suction/blowing *International Communications in Heat and Mass Transfer*, 34(3), 347–356.

Mahapatra, T. R. and Gupta, A. S. (2002). Heat transfer in stagnation point flow towards a stretching sheet, *Heat and Mass Transfer*, 38(6), 517–521

Makinde (2010) On MHD heat and mass transfer over a moving vertical plate with a convective surface boundary condition. *The Canadian Journal of Chemical Engineering* 88 (6), 983-990

Malvandi.AHedayati.F, Ganji.D.D (2016) Slip effects on unsteady stagnation point flow of a nanofluid over a stretching sheet. *Powder Technology* Volume 253, Pages 377–384

Mohd H. M. Y., Anuar I. and Ioan P. (2015). MHD Stagnation-Point Flow and Heat Transfer with Effects of Viscous Dissipation, Joule Heating and Partial Velocity Slip *Sci Rep.* 2016;6:31607. Published online 2016 Aug 16. doi: 10.1038/srep31607 PMID: PMC4985843.

Mukhopadhyay, S. and Gorla, R. S. R. (2012). Effects of partial slip on boundary layer flow past a permeable exponential stretching sheet in presence of thermal radiation, *Heat and Mass Transfer*, 48(10), 1773–1781.



- Mukhopadhyay, S., De, P. R., Bhattacharyya, K. and Layek, G. C. (2012). Slip effects on mixed convection flow along a stretching cylinder, *International Journal of Heat and Technology*, 30(2), 19–24.
- Mukhopadhyay, S. (2011). Effects of slip on unsteady mixed convective flow and heat transfer past a porous stretching surface, *Nuclear Engineering and Design*, 241(8), 2660–2665.
- Nazar, R., Amin, N., Filip, D. and Pop, I. (2004). Unsteady boundary layer flow in the region of the stagnation point on a stretching sheet, *International Journal of Engineering Science*, vol. 42, number 11-12, 1241–1253.
- Nik L. N. M. A., Koo, L. F., Wong, T. J. and Suali, M. (2013). Mixed convection boundary layers with prescribed temperature in the unsteady stagnation point flow toward a stretching vertical sheet, *Mathematical Problems in Engineering*, vol. 2013, Article ID195360, 10 pages.
- Nik M. A. B. N. L., Suali M., Ishak A., Arifin M. N. (2016) Unsteady Stagnation Point Flow and Heat Transfer over a Stretching/shrinking Sheet, *Journal of applied sciences* 11(20):3520 – 3524.
- Nor A. A. M., Norihan M. A., Roslinda N. and Norfifah B. (2015). Boundary Layer Stagnation-Point Slip Flow and Heat Transfer towards a Shrinking/Stretching Cylinder over a Permeable Surface. *Applied Mathematics Vol.06 No.03*,



- Ostrach, S. (1953). www.udsspace.uds.edu.gh New aspects of natural convection heat transfer. *Trans. ASME*, 75, 1287.
- Pal, D. (2009). Heat and mass transfer in stagnation-point flow towards a stretching surface in the presence of buoyancy force and thermal radiation, *Meccanica*, 44(2), 145–158.
- P L Sathyanarayanan and R Ramprabhu (2005). Study on the effect of different combinations of engine coolant additives on the heat dissipation rate of radiators, *Proc. IMechE Vol. 219 Part D: J. Automobile Engineering*, Pp. 1173 – 1179
- Sharma, P. R. and Singh, G. (2008). Unsteady flow about a stagnation point on a stretching sheet in the presence of variable free stream, *Thammasat International Journal of Science and Technology*, 13(1), 11–16.
- Sparrow, E. M., Cess, R. D. (1961). Free convection with blowing or suction. *J. Heat Tran.-Asme*, 83, 387–396.
- Stonecypher, L. (2009). Classification of fluid flow, *Bright hub engineering*.
- Tapas R. M., Samir K. N. (2016). Slip effects on unsteady stagnation-point flow and heat transfer over a shrinking sheet. *Meccanica* September 2013, Volume 48, Issue 7, pp 1599–1606
- Wang, C. Y. (2002). Flow due to a stretching boundary with partial slip—an exact solution of the Navier-Stokes equations, *Chemical Engineering Science*, 57(17), 3745–3747.



Wang, C. Y. (2006). www.udsspace.uds.edu.gh
Stagnation slip flow and heat transfer on a moving plate,
Chemical Engineering Science, 61(23), 7668–7672.

APPENDIX I

Derivation of Continuity

The partial differential equations modeling the motion of a parcel of fluid is obtained by applying the conservation law of mass to a small volume of fluid flow. Consider the mass flux through each face of the fixed infinitesimal control volume shown in

Figure A.1. Let the net flux of mass entering the element be equal to the rate of change of the mass of the element; that is,

$$\dot{m}_{in} - \dot{m}_{out} = \frac{\partial}{\partial t} m_{element} \quad (A1.1)$$

To perform this mass balance, identify ρu , ρv and ρw at the centre of the element and then treat each of these quantities as a single variable.

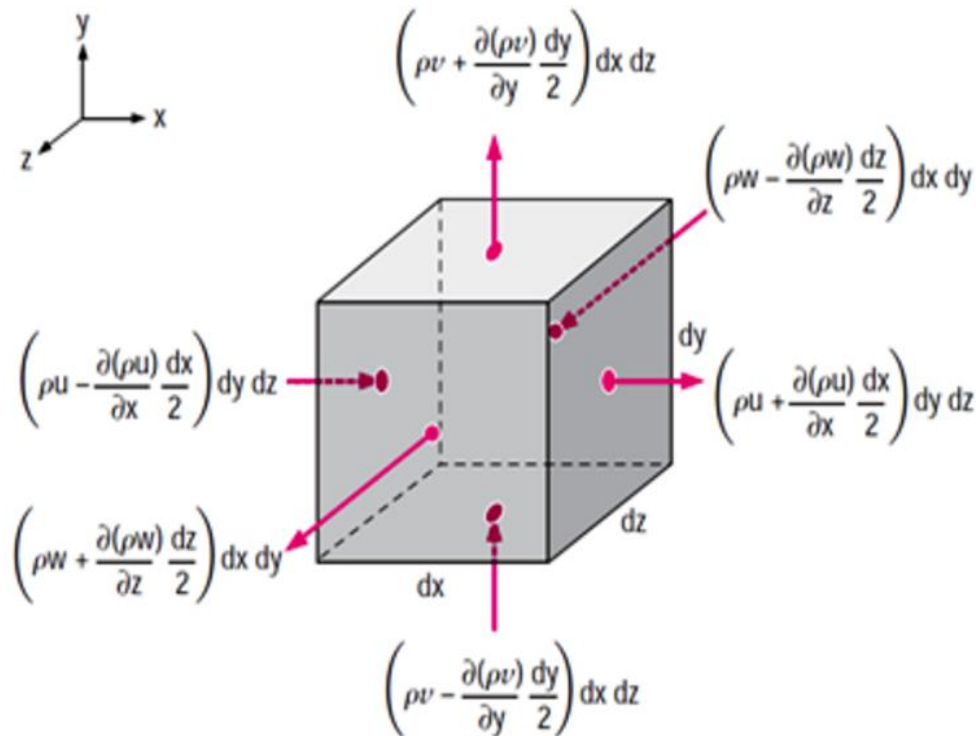


Figure A1.1 Mass flux through each of the six faces of a control volume of fluid (Çengel and Cimbala, 2006)

From **Figure A.1** which shows the mass flux through each of the six faces; Equation (A.1) takes the form

$$\left[\rho u - \frac{\partial(\rho u)}{\partial x} \frac{dx}{2} \right] dy dz - \left[\rho u + \frac{\partial(\rho u)}{\partial x} \frac{dx}{2} \right] dy dz + \left[\rho v - \frac{\partial(\rho v)}{\partial y} \frac{dy}{2} \right] dx dz - \left[\rho v + \frac{\partial(\rho v)}{\partial y} \frac{dy}{2} \right] dx dz$$



$$+ \left[\rho w - \frac{\partial(\rho w)}{\partial z} \frac{dz}{2} \right] dx dy - \left[\rho w + \frac{\partial(\rho w)}{\partial z} \frac{dz}{2} \right] dx dy = \frac{\partial}{\partial t} (\rho dx dy dz) \quad (A1.2)$$

Subtracting the appropriate terms and dividing by $dx dy dz$ gives,

$$\frac{\partial(\rho u)}{\partial x} + \frac{\partial(\rho v)}{\partial y} + \frac{\partial(\rho w)}{\partial z} = -\frac{\partial \rho}{\partial t} \quad (A1.3)$$

Expanding and simplifying results in

$$\frac{\partial \rho}{\partial t} + u \frac{\partial \rho}{\partial x} + v \frac{\partial \rho}{\partial y} + w \frac{\partial \rho}{\partial z} + \rho \left(\frac{\partial u}{\partial x} + \frac{\partial v}{\partial y} + \frac{\partial w}{\partial z} \right) = 0 \quad (A1.4)$$

In terms of substantial derivative (A1.4) is written as

$$\frac{D\rho}{Dt} + \rho \left(\frac{\partial u}{\partial x} + \frac{\partial v}{\partial y} + \frac{\partial w}{\partial z} \right) = 0 \quad (A1.5)$$

This is the most general form of the differential continuity equation expressed in rectangular coordinates. Introducing the gradient operator, ∇ called “del”, which, in rectangular coordinates, is

$$\nabla = \frac{\partial}{\partial x} \hat{i} + \frac{\partial}{\partial y} \hat{j} + \frac{\partial}{\partial z} \hat{k} \quad (A1.6)$$

The continuity equation can then be written in the form

$$\frac{D\rho}{Dt} + \rho \nabla \cdot V = 0 \quad (A1.7)$$



Where $\underline{V} = u\hat{i} + v\hat{j} + w\hat{k}$ and $\nabla \cdot \underline{V}$ is called the divergence of the velocity. This form of the continuity equation does not refer to any particular coordinate system. It is the form used to express the continuity equation using various coordinate systems.



Derivation of Momentum Equation

General formulation:

The differential momentum equation is a vector equation and thus provides us with three scalar equations. There are nine stress components of the stress tensor τ_{ij} that act in a particular point in a fluid field. These stress tensors can be related to the velocity and the vector fields with the appropriate equations.

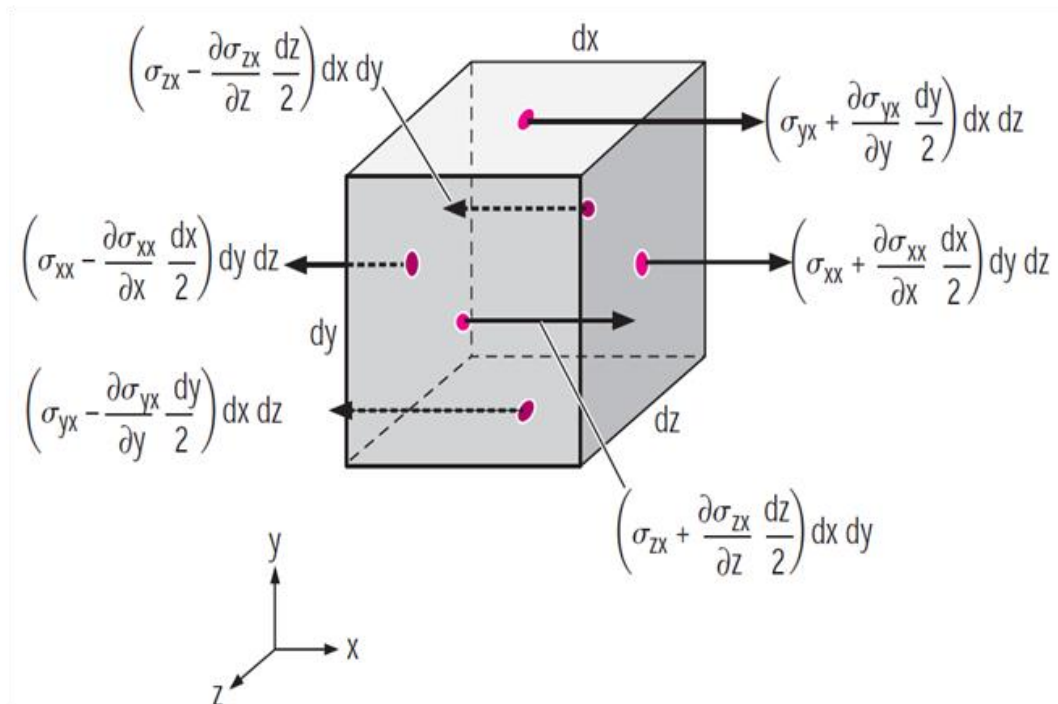


Figure A2.1 x-directional surface forces due to stress tensor component of a control volume (Çengel and Cimbala, 2006)

The stress components that act at a point are displayed on a two- and three-dimensional rectangular element in **Figure A2.1**. This element is considered to be an



exaggerated point, a cubical point; the stress components act in the positive direction on a positive face (a normal vector point in the positive coordinate direction) and in the negative direction on a negative face (a normal vector points in the negative coordinate direction). The first subscript on a stress component denotes the face, upon which the component acts, and the second subscript denotes the direction in which it acts; the component τ_{xy} acts in the positive y -direction on a positive x -face. A stress component that acts perpendicular to a face is referred to as normal stress; the components σ_{xx} , σ_{yy} and σ_{zz} are normal stresses. A stress component that acts tangential to a face is called a shear stress; the components τ_{xy} , τ_{yx} , τ_{xz} , τ_{zx} , τ_{yz} and τ_{zy} are the shear stress components. There are nine stress components that act at a particular point in a fluid. To derive the differential momentum equation, consider the forces acting on the infinitesimal fluid particle. Only forces acting on the faces are shown. The stress components are assumed to be functions of x , y , z and t ; and hence the values of the stress components change from face to face since the location of each face is slightly different. The body force is shown acting in an arbitrary direction. Newton's second law applied to a fluid particle, for the x -component direction, $\sum F_x = ma_x$. For the particle shown, it takes the form:

$$\begin{aligned} & \left[\sigma_{xx} + \frac{\partial \sigma_{xx}}{\partial x} \frac{dx}{2} \right] dydz + \left[\tau_{yx} + \frac{\partial \tau_{yx}}{\partial y} \frac{dy}{2} \right] dx dz + \left[\tau_{zx} + \frac{\partial \tau_{zx}}{\partial z} \frac{dz}{2} \right] dx dy - \left[\sigma_{xx} - \frac{\partial \sigma_{xx}}{\partial x} \frac{dx}{2} \right] dydz \\ & - \left[\tau_{yx} - \frac{\partial \tau_{yx}}{\partial y} \frac{dy}{2} \right] dx dz - \left[\tau_{zx} - \frac{\partial \tau_{zx}}{\partial z} \frac{dz}{2} \right] dx dy + \rho g_x dx dy dz = \rho dx dy dz \frac{Du}{Dt}, \quad (A2.1) \end{aligned}$$

where the component of the gravity vector g in the x -direction is g_x and $\frac{Du}{Dt}$ is the x -component acceleration of the fluid particle. Dividing by the volume $dxdydz$, (A2.1) simplifies to

$$\rho \frac{Du}{Dt} = \frac{\partial \sigma_{xx}}{\partial x} + \frac{\partial \tau_{yx}}{\partial y} + \frac{\partial \tau_{zx}}{\partial z} + \rho g_x. \quad (\text{A2.2})$$

Similarly, for y - and z -directions, we have

$$\rho \frac{Dv}{Dt} = \frac{\partial \tau_{xy}}{\partial x} + \frac{\partial \sigma_{yy}}{\partial y} + \frac{\partial \tau_{zy}}{\partial z} + \rho g_y, \quad (\text{A2.3})$$

$$\rho \frac{Dw}{Dt} = \frac{\partial \tau_{xz}}{\partial x} + \frac{\partial \tau_{yz}}{\partial y} + \frac{\partial \sigma_{zz}}{\partial z} + \rho g_z. \quad (\text{A2.4})$$

We can show by taking moments about the axes passing through the centre of the infinitesimal element, that

$$\tau_{xy} = \tau_{yx}, \tau_{xz} = \tau_{zx}, \tau_{yz} = \tau_{zy} \quad (\text{A2.5})$$

That is, from (A2.5), we say the stress tensor is symmetric; so there are actually six independent stress components. The stress tensor may be displayed in the usual way as in (A2.6)

The subscripts i and j take on numerical values 1, 2, or 3. Then τ_{12} represents the element τ_{xy} in the first row, second column.

$$\tau_{ij} = \begin{pmatrix} \sigma_{xx} & \tau_{xy} & \tau_{xz} \\ \tau_{yx} & \sigma_{yy} & \tau_{yz} \\ \tau_{zx} & \tau_{zy} & \sigma_{zz} \end{pmatrix} \quad (\text{A2.6})$$



The Navier – Stokes Equations

Many fluids exhibit a linear relationship between the stress components and the velocity gradients. Such fluids are called Newtonian fluids and include common fluids such as water, oil, and air. If in addition to linearity, we require that the fluid be isotropic, it is possible to relate the stress components and the velocity gradients using only two fluid properties, the viscosity μ and the second coefficient of viscosity λ . The stress-velocity gradient relations, often referred to as the constitutive equations, are stated as follows:

$$\sigma_{xx} = -p + 2\mu \frac{\partial u}{\partial x} + \lambda \nabla \cdot V, \tau_{xy} = \mu \left(\frac{\partial u}{\partial y} + \frac{\partial v}{\partial x} \right), \sigma_{yy} = -p + 2\mu \frac{\partial v}{\partial y} + \lambda \nabla \cdot V, \\ \tau_{xz} = \mu \left(\frac{\partial u}{\partial z} + \frac{\partial w}{\partial x} \right), \quad (A2.7)$$

$$\sigma_{zz} = -p + 2\mu \frac{\partial w}{\partial z} + \lambda \nabla \cdot V, \tau_{yz} = \mu \left(\frac{\partial v}{\partial z} + \frac{\partial w}{\partial y} \right).$$

For most gases and for monatomic gases exactly, the second coefficient of viscosity is related to the viscosity by

$$\lambda = -\frac{2}{3} \mu, \quad (A2.8)$$

a condition that is known as Stokes' hypothesis. With this relationship, the negative average of the three normal stresses is equal to the pressure, that is,

$$-\frac{1}{3}(\sigma_{xx} + \sigma_{yy} + \sigma_{zz}) = p. \quad (A2.9)$$



Using (A2.7), this can be shown to always be true for a liquid in which $\nabla \cdot V = 0$, and with Stokes' hypothesis, it is also true for a gas. If the constitutive equations are substituted into the differential momentum equations (A2.2), (A2.3), and (A2.4), give

$$\rho \frac{Du}{Dt} = -\frac{\partial p}{\partial x} + \rho g_x + \mu \left(\frac{\partial^2 u}{\partial x^2} + \frac{\partial^2 u}{\partial y^2} + \frac{\partial^2 u}{\partial z^2} \right) + \frac{\mu}{3} \frac{\partial}{\partial x} \left(\frac{\partial u}{\partial x} + \frac{\partial v}{\partial y} + \frac{\partial w}{\partial z} \right), \quad (\text{A2.10})$$

$$\rho \frac{Dv}{Dt} = -\frac{\partial p}{\partial y} + \rho g_y + \mu \left(\frac{\partial^2 v}{\partial x^2} + \frac{\partial^2 v}{\partial y^2} + \frac{\partial^2 v}{\partial z^2} \right) + \frac{\mu}{3} \frac{\partial}{\partial y} \left(\frac{\partial u}{\partial x} + \frac{\partial v}{\partial y} + \frac{\partial w}{\partial z} \right), \quad (\text{A2.11})$$

$$\rho \frac{Dw}{Dt} = -\frac{\partial p}{\partial z} + \rho g_z + \mu \left(\frac{\partial^2 w}{\partial x^2} + \frac{\partial^2 w}{\partial y^2} + \frac{\partial^2 w}{\partial z^2} \right) + \frac{\mu}{3} \frac{\partial}{\partial z} \left(\frac{\partial u}{\partial x} + \frac{\partial v}{\partial y} + \frac{\partial w}{\partial z} \right), \quad (\text{A2.12})$$

where a homogeneous fluid is assumed. That is, the fluid properties (for example, the viscosity) are independent of position. For an incompressible flow, the continuity equation allows the equations above to be reduced to

$$\rho \frac{Du}{Dt} = -\frac{\partial p}{\partial x} + \rho g_x + \mu \left(\frac{\partial^2 u}{\partial x^2} + \frac{\partial^2 u}{\partial y^2} + \frac{\partial^2 u}{\partial z^2} \right) \quad (\text{A2.13})$$

$$\rho \frac{Dv}{Dt} = -\frac{\partial p}{\partial y} + \rho g_y + \mu \left(\frac{\partial^2 v}{\partial x^2} + \frac{\partial^2 v}{\partial y^2} + \frac{\partial^2 v}{\partial z^2} \right) \quad (\text{A2.14})$$

$$\rho \frac{Dw}{Dt} = -\frac{\partial p}{\partial z} + \rho g_z + \mu \left(\frac{\partial^2 w}{\partial x^2} + \frac{\partial^2 w}{\partial y^2} + \frac{\partial^2 w}{\partial z^2} \right) \quad (\text{A2.15})$$

These are the Navier-Stokes Equations, named after Louis M. H. Navier (1785-1836) and George Stokes (1819-1903).

$$\rho \frac{DV}{Dt} = -\nabla p + \rho g + \mu \nabla^2 V \quad (\text{A2.16})$$



Derivation of the Energy Equation

Consider the infinitesimal fluid element, shown in **Figure A2.1**. The heat transfer rate \dot{Q} through an area A is given by Fourier's law of heat transfer, named after Jean (1768-1830):

$$\dot{Q} = -\kappa A \frac{\partial T}{\partial n}, \quad (\text{A3.1})$$

where n is the direction normal to the area, T is the temperature, and κ is the thermal conductivity, assumed to be constant. The rate of work done by a force is the magnitude of the force multiplied by the velocity in the direction of the force, that is,

$$\dot{W} = pAV, \quad (\text{A3.2})$$

where V is the velocity in the direction of the pressure force pA . The first law of thermodynamics applied to a fluid particle can be written as

$$\dot{Q} - \dot{W} = \frac{DE}{Dt}, \quad (\text{A3.3})$$

where D/Dt is used since we are following a fluid particle at the instant shown.

$$\kappa dydz \left(\left. \frac{\partial T}{\partial x} \right|_{x+dx} - \left. \frac{\partial T}{\partial x} \right|_x \right) - \frac{\partial}{\partial x} (pu) dx dy dz + \kappa dx dz \left(\left. \frac{\partial T}{\partial y} \right|_{y+dy} - \left. \frac{\partial T}{\partial y} \right|_y \right) - \frac{\partial}{\partial y} (pv) dx dy dz$$



$$+ \kappa dx dy \left(\frac{\partial T}{\partial z} \Big|_{z+dz} - \frac{\partial T}{\partial z} \Big|_z \right) - \frac{\partial}{\partial z} (pw) dx dy dz = \rho dx dy dz \frac{D}{Dt} \left(\frac{u^2 + v^2 + w^2}{2} + gz + \tilde{u} \right), \quad (\text{A3.4})$$

where \tilde{u} is the internal energy, E has included kinetic, potential and internal energy, and the z -axis is assumed vertical. Also, since the mass of a fluid particle is constant $\rho dx dy dz$ is outside the D/Dt -operator. Divide both sides by $dx dy dz$. The result is

$$\kappa \left(\frac{\partial^2 T}{\partial x^2} + \frac{\partial^2 T}{\partial y^2} + \frac{\partial^2 T}{\partial z^2} \right) - \frac{\partial}{\partial x} (pu) - \frac{\partial}{\partial y} (pv) - \frac{\partial}{\partial z} (pw) = \rho \frac{D}{Dt} \left(\frac{u^2 + v^2 + w^2}{2} + gz + \tilde{u} \right). \quad (\text{A3.5})$$

This can be rearranged as follows:

$$\begin{aligned} & \kappa \left(\frac{\partial^2 T}{\partial x^2} + \frac{\partial^2 T}{\partial y^2} + \frac{\partial^2 T}{\partial z^2} \right) - p \left(\frac{\partial u}{\partial x} + \frac{\partial v}{\partial y} + \frac{\partial w}{\partial z} \right) - u \frac{\partial p}{\partial x} - v \frac{\partial p}{\partial y} \\ & - w \frac{\partial p}{\partial z} = \rho u \frac{Du}{Dt} + \rho v \frac{Dv}{Dt} + \rho w \frac{Dw}{Dt} + \rho g \frac{Dz}{Dt} + \rho \frac{D\tilde{u}}{Dt}. \quad (\text{A3.6}) \end{aligned}$$

The Euler's equations are applicable for this inviscid flow. Hence, the last three terms on the left equal the first four terms on the right if we recognize that

$$\frac{Dz}{Dt} = \frac{\partial z}{\partial t} + u \frac{\partial z}{\partial x} + v \frac{\partial z}{\partial y} + w \frac{\partial z}{\partial z} = w, \quad (\text{A3.7})$$

since x , y , z and t are all independent variables. The simplified energy equation then takes the form

$$\rho \frac{D\tilde{u}}{Dt} = \kappa \left(\frac{\partial^2 T}{\partial x^2} + \frac{\partial^2 T}{\partial y^2} + \frac{\partial^2 T}{\partial z^2} \right) - p \left(\frac{\partial u}{\partial x} + \frac{\partial v}{\partial y} + \frac{\partial w}{\partial z} \right). \quad (\text{A3.8})$$

In vector form, this is expressed as



$$\rho \frac{D\tilde{u}}{Dt} = \kappa \nabla^2 T - p \nabla \cdot V \quad (\text{A3.9})$$

Before simplifying this equation for incompressible gas flow, it could be written in terms of enthalpy rather than internal energy. Using

$$\tilde{u} = h - \frac{P}{\rho}. \quad (\text{A3.10})$$

The energy equation now becomes

$$\rho \frac{Dh}{Dt} = \kappa \nabla^2 T + \frac{Dp}{Dt}. \quad (\text{A3.11})$$

Two special cases can be considered. First, for a liquid flow, the continuity equation requires that $\nabla \cdot V = 0$ and with $\tilde{u} = c_p T$, c_p being the specific heat capacity at constant pressure. Equation (A3.9) becomes

$$\frac{DT}{Dt} = \alpha \nabla^2 T \quad (\text{A3.12})$$

In (A3.12) we have introduced the thermal diffusivity defined by

$$\alpha = \frac{\kappa}{\rho c_p} \quad (\text{A3.13})$$

If viscous effects are not negligible, the derivation would include the work input due to the shear stress components. This would add a term to the right-hand side of all the differential energy equations above; this term is called the dissipation function Φ , which, in rectangular coordinates, is



$$\Phi = 2\mu \left[\left(\frac{\partial u}{\partial x} \right)^2 + \left(\frac{\partial v}{\partial y} \right)^2 + \left(\frac{\partial w}{\partial z} \right)^2 + \frac{1}{2} \left(\frac{\partial u}{\partial y} + \frac{\partial v}{\partial x} \right)^2 + \frac{1}{2} \left(\frac{\partial v}{\partial z} + \frac{\partial w}{\partial y} \right)^2 + \frac{1}{2} \left(\frac{\partial u}{\partial z} + \frac{\partial w}{\partial x} \right)^2 \right] \quad (\text{A3.14})$$

Therefore, the energy equation for incompressible fluid flow becomes

$$\frac{DT}{Dt} = \alpha \Delta^2 T + \Phi \quad (\text{A3.15})$$

In equation (A3.15), the left hand represents the convective term whilst the right hand side are respectively, the rate of heat diffusion to the fluid particles and the rate of viscous dissipation per unit volume.



Derivation of the Concentration Equation

The concentration equation is derived on the principles of species conservation in a mixture. In addition to accounting for the convection and diffusion of each species, we must allow the possibility that a species may be created or destroyed by chemical reactions occurring in the bulk medium (homogeneous reactions). Reactions on surfaces surrounding the medium (heterogeneous reactions) must be accounted for in the boundary conditions

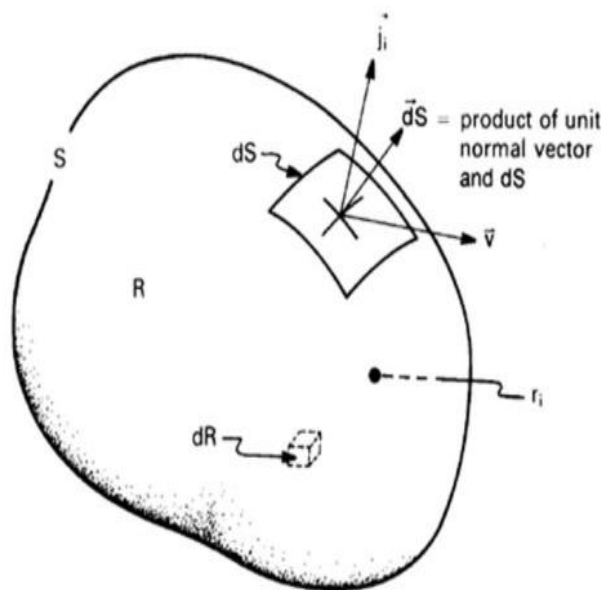


Figure A4.1 A Control volume in a fluid-flow and mass-diffusion field (Lienhard IV and Lienhard, 2008)

Consider, in the usual way, an arbitrary control volume, R , with a boundary, S , as shown in Fig A4.1. The control volume is fixed in space, with fluid moving through



it. Species i may accumulate in R , it may travel in and out of R by bulk convection or by diffusion, and it may be created within R by homogeneous reactions. The rate of creation species i is denoted by \dot{r}_i ; and, because chemical reaction conserve mass, the net mass reaction is $\dot{r} = \sum \dot{r}_i = 0$. The rate of change of the mass of species i in R is then described by the following balance:

$$\frac{d}{dt} \int_R \rho_i dR = - \int_S \bar{n}_i \cdot d\bar{S} + \int_R \dot{r}_i dR \quad (\text{A4.1})$$

$$\frac{d}{dt} \int_R \rho_i dR = - \int_S \rho_i \bar{v} \cdot d\bar{S} - \int_S \bar{j}_i \cdot d\bar{S} + \int_R \dot{r}_i dR \quad (\text{A4.2})$$

The term on the left hand side of equation (A4.2) is the rate of increase of the species in the control volume and the terms on the right hand side depicts respectively, the rate of convection of the species out of the control volume; the diffusion of the species out of the control volume; and the rate of creation of the species in the control volume.

This species conservation statement is identical to the energy conservation statement except that the mass of the species has taken the place of energy and heat. The surface integral may be converted to volume integrals using Gauss' theorem and rearranged to appear as:

$$\int_R \left[\frac{\partial \rho_i}{\partial t} + \nabla \cdot (\rho_i \bar{v}) + \nabla \cdot \bar{j}_i - \dot{r}_i \right] = 0 \quad (\text{A4.3})$$

Since the control volume is selected arbitrarily, the integrand must be identically zero.

Thus, the general form of the species conservation equation becomes:



$$\frac{\partial \rho_i}{\partial t} + \nabla \cdot (\rho_i \bar{v}) = -\nabla \cdot \bar{j}_i + \dot{r}_i \quad (\text{A4.4})$$

The mass conservation equation for the entire mixture can be obtained by summing equation (A4.4) over the species region and apply the requirement that there be no net creation of mass:

$$\sum_i \left[\frac{\partial \rho_i}{\partial t} + \nabla \cdot (\rho_i \bar{v}) \right] = \sum_i [-\nabla \cdot \bar{j}_i + \dot{r}_i] \quad (\text{A4.5})$$

$$\text{So that,} \quad \frac{\partial \rho}{\partial t} + \nabla \cdot (\rho \bar{v}) = 0 \quad (\text{A4.6})$$

Equation (A4.6) applies to any mixture, including those with varying density.

Incompressible Mixtures

For an incompressible mixture, $\nabla \cdot \bar{v} = 0$ and the second term in equation (A4.6) may be written as

$$\nabla \cdot (\rho \bar{v}) = \bar{v} \cdot \nabla \rho_i + \rho_i \cdot \nabla \bar{v} = \bar{v} \cdot \nabla \rho_i \quad (\text{A4.7})$$

Comparing the resulting incompressible species equation to the incompressible energy equation:

$$\frac{\partial \rho_i}{\partial t} + \bar{v} \cdot \nabla \rho_i = -\nabla \cdot \bar{j}_i + \dot{r}_i \quad (\text{A4.8})$$

$$\rho c_p \left(\frac{\partial T}{\partial t} + \bar{v} \cdot \nabla T \right) = -\nabla \cdot \bar{q} + \dot{q} \quad (\text{A4.9})$$



the reaction term, \dot{r}_i , is analogous to the heat generation term, \dot{q} ; the diffusion flux, \vec{j}_i , is analogous to the heat flux, \vec{q} , and $d\rho_i$ is analogous to $\rho c_p dT$.

The Fick's Law

The Fick's Law states that during mass diffusion, the flux, \vec{j}_i of a dilute component, 1, into a second fluid, 2, is proportional to the gradient of its mass concentration, m_1 .

Thus

$$\vec{j}_i = -\rho D_{12} \nabla m_1, \quad (\text{A4.10})$$

where the constant D_{12} is the binary diffusion coefficient.

We can use Equation (A4.10) to eliminate \vec{j}_i in equation (A4.8). The resulting equation may be written in different forms depending on what is assumed about the variation of the physical properties. If the product ρD_{im} is spatially uniform, then equation (A4.8) becomes:

$$\frac{D}{Dt} m_i = D_{im} \nabla^2 m_i + \frac{\dot{r}_i}{\rho} \quad (\text{A4.11})$$

If instead, ρ and D_{im} are both spatially uniform, then,

$$\frac{D}{Dt} \rho_i = D_{im} \nabla^2 \rho_i + \dot{r}_i \quad (\text{A4.12})$$

We now state the equation of species conservation and its particular form in molar variables instead of the mass variables as,



$$\frac{DC}{Dt} = D\nabla^2 C + \dot{r}, \quad (\text{A4.13})$$

where C is the species concentration, D is the mass diffusivity and \dot{r} is the rate of generation of species.



MAPLE CODE FOR NUMERICAL RESULTS

```
> Pr := 0.72 : M := 0.1 : Sc := 0.24 : beta := 0.1 : Ra := 0.1 : Br := 0.1 :  
Bi := 0.1 :
```

```
fcns := {F(y), theta(y), phi(y)} :
```

```
sys1 := diff(F(y), y$3) + 1/2 * F(y) * diff(F(y), y$2) - M  
      * (diff(F(y), y) - 1) = 0, (1 + 4/3 * (Ra)) * diff(theta(y), y$2)  
      + 1/2 * Pr * F(y) * diff(theta(y), y) + Br * (diff(F(y), y$2))^2 + Br  
      * M * (diff(F(y), y) - 1)^2 = 0, diff(phi(y), y$2) + 1/2 * Sc * F(y)  
      * diff(phi(y), y) - Sc * beta * phi(y) = 0, D(F)(0) = 0, F(0) = 0,  
      D(theta)(0) = Bi * (theta(0) - 1), phi(0) = 1, D(F)(10) = 1, theta(10) = 0,  
      phi(10) = 0 :
```

```
dy^3 F(y) + 1/2 F(y) (dy^2 F(y)) - 0.1 (dy F(y)) + 0.1 = 0,  
1.133333333 (dy^2 theta(y)) + 0.3600000000 F(y) (dy theta(y))  
+ 0.1 (dy^2 F(y))^2 + 0.01 (dy F(y) - 1)^2 = 0, dy^2 phi(y)  
+ 0.1200000000 F(y) (dy phi(y)) - 0.024 phi(y) = 0, D(F)(0)  
= 0, F(0) = 0, D(theta)(0) = 0.1 theta(0) - 0.1, phi(0) = 1, D(F)(10)  
= 1, theta(10) = 0, phi(10) = 0
```

```
p := dsolve({sys1, D(F)(0) = 0, F(0) = 0, D(theta)(0) = Bi * (theta(0)  
- 1), phi(0) = 1, D(F)(10) = 1, theta(10) = 0, phi(10) = 0}, fcns, type  
= numeric, method = bvp, abserr = 1e-6)
```

```
proc(x_bvp) ... end proc
```

```
dsol1 := dsolve({sys1}, numeric, output = operator)
```





www.udsspace.uds.edu.gh

```

[y = proc(y) ... end proc, F = proc(y) ... end proc, D(F) =
  proc(y)
  ...
end proc, D(2)(F) = proc(y) ... end proc, ϕ = proc(y)
  ...
end proc, D(ϕ) = proc(y) ... end proc, θ = proc(y) ... end proc,
  D(θ) = proc(y) ... end proc]

dsol1(0);
[y = 0, F(0) = 0., D(F)(0) = 0., D(2)(F)(0)
  = 0.451835091240999020ϕ(0) = 0.9999999999999956D(ϕ)(0)
  = -0.24858613612211488ϕ(0) = 0.315846615504484674
  D(θ)(0) = -0.068415338449551499]
  
```

MAPLE CODE FOR GRAPHICAL RESULTS

```

> with(plots) :
Pr := 0.72 : M := 0.1 : Sc := 0.24 : β := 0.1 : Ra := 0.1 : Br := 0.1 :
Bi := 0.1 :

fcns := {F(y), θ(y), φ(y)} :
sys := diff(F(y), y$3) + 1/2 · F(y) · diff(F(y), y$2) - M
      · (diff(F(y), y) - 1) = 0, (1 + 4/3 · (Ra)) · diff(θ(y), y$2)
      + 1/2 · Pr · F(y) · diff(θ(y), y) + Br · (diff(F(y), y$2))^2 + Br
      · M · (diff(F(y), y) - 1)^2 = 0, diff(φ(y), y$2) + 1/2 · Sc · F(y)
      · diff(φ(y), y) - Sc · β · φ(y) = 0 :

p1 := dsolve({sys, D(F)(0) = 0, F(0) = 0, D(θ)(0) = Bi · (θ(0)
      - 1), φ(0) = 1, D(F)(10) = 1, θ(10) = 0, φ(10) = 0}, fcns, type
      = numeric, method = bvp, abserr = 1e-6)

proc(x_bvp) ... end proc

p1f := odeplot(p1, [y, F'(y)], 0..10, numpoints = 50, labels = ["y",
      "velocity"], style = patch, symbol = asterisk, color = black) :

p1t := odeplot(p1, [y, θ(y)], 0..10, numpoints = 50, labels = ["y",
      "Temperature"], style = patch, symbol = asterisk, color = black) :

p1c := odeplot(p1, [y, φ(y)], 0..10, numpoints = 50, labels = ["y",
      "concentration"], style = patch, symbol = asterisk, color = black) :

with(plots) :
Pr := 1 : M := 0.1 : Sc := 0.24 : β := 0.1 : Ra := 0.1 : Br := 0.1 : Bi
:= 0.1 :

fcns := {F(y), θ(y), φ(y)} :
sys := diff(F(y), y$3) + 1/2 · F(y) · diff(F(y), y$2) - M
      · (diff(F(y), y) - 1) = 0, (1 + 4/3 · (Ra)) · diff(θ(y), y$2)
      + 1/2 · Pr · F(y) · diff(θ(y), y) + Br · (diff(F(y), y$2))^2 + Br
      · M · (diff(F(y), y) - 1)^2 = 0, diff(φ(y), y$2) + 1/2 · Sc · F(y)
      · diff(φ(y), y) - Sc · β · φ(y) = 0 :

```




```
p2 := dsolve( {sys, D(F)(0) = 0, F(0) = 0, D(θ)(0) = Bi·(θ(0)
    - 1), φ(0) = 1, D(F)(10) = 1, θ(10) = 0, φ(10) = 0}, fcns, type
    = numeric, method = bvp, abserr = 1e-6)
```

```
proc(x_bvp) ... end proc
```

```
p2f := odeplot(p2, [y, F'(y)], 0..10, numpoints = 50, labels = ["y",
    "velocity"], style = point, symbol = circle, color = black) :
```

```
p2t := odeplot(p2, [y, θ(y)], 0..10, numpoints = 50, labels = ["y",
    "Temperature"], style = point, symbol = circle, color = black) :
```

```
p2c := odeplot(p2, [y, φ(y)], 0..10, numpoints = 50, labels = ["y",
    "concentration"], style = point, symbol = circle, color = black) :
```

```
with(plots) :
```

```
Pr := 4 : M := 0.1 : Sc := 0.24 : β := 0.1 : Ra := 0.1 : Br := 0.1 : Bi
    := 0.1 :
```

```
fcns := {F(y), θ(y), φ(y)} :
```

```
sys := diff(F(y), y$3) +  $\frac{1}{2} \cdot F(y) \cdot \text{diff}(F(y), y$2) - M$ 
    · (diff(F(y), y) - 1) = 0,  $\left(1 + \frac{4}{3} \cdot (Ra)\right) \cdot \text{diff}(\theta(y), y$2)$ 
    +  $\frac{1}{2} \cdot Pr \cdot F(y) \cdot \text{diff}(\theta(y), y) + Br \cdot (\text{diff}(F(y), y$2))^2 + Br$ 
    ·  $M \cdot (\text{diff}(F(y), y) - 1)^2 = 0, \text{diff}(\phi(y), y$2) + \frac{1}{2} \cdot Sc \cdot F(y)$ 
    ·  $\text{diff}(\phi(y), y) - Sc \cdot \beta \cdot \phi(y) = 0 :$ 
```

```
p3 := dsolve( {sys, D(F)(0) = 0, F(0) = 0, D(θ)(0) = Bi·(θ(0)
    - 1), φ(0) = 1, D(F)(10) = 1, θ(10) = 0, φ(10) = 0}, fcns, type
    = numeric, method = bvp, abserr = 1e-6)
```

```
proc(x_bvp) ... end proc
```

```
p3f := odeplot(p3, [y, F'(y)], 0..10, numpoints = 50, labels = ["y",
    "velocity"], style = point, symbol = point, color = black) :
```

```
p3t := odeplot(p3, [y, θ(y)], 0..10, numpoints = 50, labels = ["y",
    "Temperature"], style = point, symbol = point, color = black) :
```

```
p3c := odeplot(p3, [y, φ(y)], 0..10, numpoints = 50, labels = ["y",
    "concentration"], style = point, symbol = point, color = black) :
```

```
with(plots) :
```

```
Pr := 7.1 : M := 0.1 : Sc := 0.24 : β := 0.1 : Ra := 0.1 : Br := 0.1 :
    Bi := 0.1 :
```

```
fcns := {F(y), θ(y), φ(y)} :
```



www.udsspace.uds.edu.gh

```
sys := diff(F(y), y$3) + 1/2 * F(y) * diff(F(y), y$2) - M
      * (diff(F(y), y) - 1) = 0, (1 + 4/3 * (Ra)) * diff(theta(y), y$2)
      + 1/2 * Pr * F(y) * diff(theta(y), y) + Br * (diff(F(y), y$2))^2 + Br
      * M * (diff(F(y), y) - 1)^2 = 0, diff(phi(y), y$2) + 1/2 * Sc * F(y)
      * diff(phi(y), y) - Sc * beta * phi(y) = 0 :

p4 := dsolve({sys, D(F)(0) = 0, F(0) = 0, D(theta)(0) = Bi * (theta(0)
      - 1), phi(0) = 1, D(F)(10) = 1, theta(10) = 0, phi(10) = 0}, fcns, type
      = numeric, method = bvp, abserr = 1e-6)
```

proc(x_bvp) ... end proc

```
p4f := odeplot(p4, [y, F'(y)], 0..10, numpoints = 50, labels = ["y",
      "velocity"], style = point, symbol = cross, color = black) :

p4t := odeplot(p4, [y, theta(y)], 0..10, numpoints = 50, labels = ["y",
      "Temperature"], style = point, symbol = cross, color = black) :

> p4c := odeplot(p4, [y, phi(y)], 0..10, numpoints = 50, labels = ["y",
      "concentration"], style = point, symbol = cross, color = black) :
```



The Runge-Kutta (RK) Method

The Runge-Kutta (RK) method is based on the Taylor series expansion formulae, but yield in general better algorithms for solutions of an ODE. The basic philosophy is that it provides an intermediate step in the computation of y_{i+1} .

To see this, consider first the following definitions

$$\frac{dy}{dt} = f(t, y), (A10.1)$$

$$y(t) = \int f(t, y) dt, (A10.2)$$

$$y_{i+1} = y_i + \int_{t_i}^{t_{i+1}} f(t, y) dt. (A10.3)$$

To demonstrate the philosophy behind RK methods, let us consider the second-order RK method, RK2. The first approximation consists in Taylor expanding $f(t, y)$ around the centre of the integration interval t_i to t_{i+1} , i.e., at $t_i + h/2$, h being the step. Using the midpoint formula for an integral, defining $y(t_i + h/2) = y_{i+1/2}$ and $t_i + h/2 = t_{i+1/2}$, we obtain

$$\int_{t_i}^{t_{i+1}} f(t, y) dt \approx hf(t_{i+1/2}, y_{i+1/2}) + O(h^3) (A10.4)$$

This means in turn that we have



$$y_{i+1} = y_i + hf(t_{i+1/2}, y_{i+1/2}) + O(h^3) \quad (\text{A10.5})$$

However, we do not know the value of $y_{i+1/2}$. Here comes thus the next approximation, namely, we use Euler's method to approximate $y_{i+1/2}$. We have then

$$y_{(i+1/2)} = y_i + \frac{h}{2} \frac{dy}{dh} = y(t_i) + \frac{h}{2} f(t_i, y_i) \quad (\text{A10.6})$$

This means that we can define the following algorithm for the second-order Runge-Kutta method, RK2.

$$k_1 = hf(t_i, y_i) \quad (\text{A10.7})$$

$$k_2 = hf(t_{i+1/2}, y_i + k_1/2) \quad (\text{A10.8})$$

$$y_{i+1} \approx y_i + k_2 + O(h^3) \quad (\text{A10.9})$$

The difference between the previous one-step methods is that we now need an intermediate step in our evaluation, namely $t_i + h/2 = t_{(i+1/2)}$ where we evaluate the derivative f . This involves more operations, but the gain is a better stability in the solution. The fourth-order Runge-Kutta, RK4, which we will employ in the solution of various differential equations below, is easily derived. The steps are as follows. We start again with (A10.7), but instead of approximating the integral with the midpoint rule, we use now Simpson's rule at $t_i + h/2$, with h being the step. Using Simpson's formula for an integral, defining $y(t_i + h/2) = y_{i+1/2}$ and $t_i + h/2 = t_{i+1/2}$, we obtain

$$\int_{t_i}^{t_{i+1}} f(t, y) dt \approx \frac{h}{6} \left[f(t_i, y_i) + 4f(t_{i+1/2}, y_{i+1/2}) + f(t_{i+1}, y_{i+1}) \right] + O(h^5) \quad (\text{A10.11})$$



This means;

$$y_{i+1} = y_i + \frac{h}{6} \left[f(t_i, y_i) + 4f\left(t_{i+1/2}, y_{i+1/2}\right) + f(t_{i+1}, y_{i+1}) \right] + O(h^5) \quad (A10.12)$$

However, we do not know the values of $y_{i+1/2}$ and y_{i+1} . The fourth-order Runge-Kutta method splits the midpoint evaluations in two steps, that is we have

$$y_{i+1} \approx y_i + \frac{h}{6} \left[f(t_i, y_i) + 2f\left(t_{i+1/2}, y_{i+1/2}\right) + 2f\left(t_{i+1/2}, y_{i+1/2}\right) + f(t_{i+1}, y_{i+1}) \right] \quad (A10.13)$$

since we want to approximate the slope at $y_{i+1/2}$ in two steps. The first two function evaluations are as for the second order Runge-Kutta method. Thus, the algorithm consists in first calculating k_1 with t_i , y_1 and f as inputs. Thereafter, we increase the step size by $h/2$ and calculate k_2 , then k_3 and finally k_4 . With this caveat, we can then obtain the new value for the variable y . It results in four function evaluations, but the accuracy is increased by two orders compared with the second-order Runge-Kutta method. The fourth order Runge-Kutta method has a global truncation error which goes like $O(h^4)$.



Shooting method

In many physics applications we encounter differential equations like

$$\frac{d^2y}{dx^2} + k^2(x)y = F(x); \quad a \leq x \leq b, \quad (A11.1)$$

with boundary conditions

$$y(a) = \alpha, y(b) = \beta. \quad (A11.2)$$

We can interpret $F(x)$ as an inhomogeneous driving force while $k(x)$ is a real function. If it is positive the solutions $y(x)$ will be oscillatory functions, and if negative they are exponentially growing or decaying functions. To solve this equation we could start with for example the Runge-Kutta method or various improvements to Euler's method, as discussed in the previous chapter. Then we would need to transform this equation to a set of coupled first-order equations. We could however start with the discretized version for the second derivative. We discretize our equation and introduce a step length $h = (b-a)/N$, with N being the number of equally spaced mesh points. Our discretized second derivative reads at a step $x_i = a + ih$ with $i = 0, 1, \dots$

$$y''_i = y_i + \frac{y_{i+1} + y_{i-1} - 2y_i}{h^2} + O(h^2), \quad (A11.3)$$

leading to a discretized differential equation:



$$F_i = k_i^2 y_i + \frac{y_{i+1} + y_{i-1} - 2y_i}{h^2} + O(h^2). \quad (A11.4)$$

Recall that the fourth-order Runge-Kutta method has a local error of $O(h^4)$. Since we want to integrate our equation from $x_0 = a$ to $x_N = b$, we rewrite it as

$$y_{i+1} \approx -y_{i-1} + y_i (2 - h^2 k_i^2 + h^2 F_i). \quad (A11.5)$$

Starting at $i = 1$ we have after one step:

$$y_2 \approx -y_0 + y_1 (2 - h^2 k_1^2 + h^2 F_1). \quad (A11.6)$$

Irrespective of method to approximate the second derivative, this equation uncovers our first problem. While $y_0 = y(a) = 0$, our function value y_1 is unknown, unless we have an analytic expression for $y(x)$ at $x = 0$. Knowing y_1 is equivalent to knowing y' at $x = 0$ since the first derivative is given by

$$y'_i \approx \frac{y_{i+1} - y_i}{h}. \quad (A11.7)$$

